Picosecond solvation dynamics of coumarin 153: The importance of molecular aspects of solvation

Mark Maroncelli and Graham R. Fleming

Citation: The Journal of Chemical Physics **86**, 6221 (1987); doi: 10.1063/1.452460
View online: http://dx.doi.org/10.1063/1.452460
View Table of Contents: http://scitation.aip.org/content/aip/journal/jcp/86/11?ver=pdfcov
Published by the AIP Publishing

Picosecond solvation dynamics of coumarin 153: The importance of molecular aspects of solvation

Mark Maroncelli and Graham R. Fleming
Department of Chemistry, The University of Chicago, Chicago, Illinois 60637

(Received 7 January 1987; accepted 24 February 1987)

Solvation dynamics in polar liquids have been examined using the probe molecule coumarin 153 (Cu153) and picosecond spectroscopic techniques. Steady-state absorption and fluorescence spectra of Cu153 as a function of solvent show that the frequency of the electronic spectrum of this probe provides a convenient measure of solvation energetics. Both nonspecific dipolar and to a smaller degree H-bonding solute–solvent interactions are involved. Time-correlated single photon counting was used to observe time-dependent shifts of the fluorescence spectrum of Cu153 in a variety of alcohols, propylene carbonate, and *N*-methylpropionamide solvents as a function of temperature. These time-dependent spectral shifts provide a direct measure of the time dependence of the solvation process. Theoretical models that treat the solvent as a dielectric continuum do not adequately account for the observed solvation dynamics. In the solvents studied, such theories predict a single exponential shift of the fluorescence spectrum with a time constant equal to the longitudinal relaxation time (τ_L) of the solvent. We find that solvation is nonexponential in time and that the average time constant observed is, in general, greater than τ_L. As the dielectric constant of the solvent increases the disagreement between the observed and predicted solvation times becomes more pronounced. For *N*-methylpropionamide ($\epsilon_0 \sim 300$ at 245 K) solvation is observed to occur 15 times slower than predicted. These results are discussed in terms of the importance of general molecular aspects of solvation not included in a continuum description. The rotational dynamics of Cu153 in a number of polar solvents has also been examined using time-resolved fluorescence anisotropy measurements. In addition to the "normal" diffusive rotational dynamics we observe a much faster component of the anisotropy decays in polar solvents. The latter rotational component is correlated to the observed solvation time and appears to be due to rapid rotation of the transition dipole of Cu153 in response to changes in the solvent environment.

I. INTRODUCTION

Understanding how chemical reactions are modified in going from the gas phase into solution has been a theme of longstanding interest to chemists. Especially for reactions involving charged species, polar solvents can dramatically change reaction rates as well as outcomes from those which occur in the gas phase. Many of these effects can be understood with a "thermodynamic" description wherein the solvent alters the free energy surface of the reaction. For example, if reaction proceeds via a transition state which is less polar than the reactants, in a polar solvent the reactants will be stabilized relative to the transition state and the reactive barrier is increased compared with the gas phase barrier. Recent theoretical studies have pointed out that such a thermodynamic description may be inadequate in many cases.[1–5] Only if solvent motions are very fast relative to reactive motions can the solvent remain equilibrated to the reaction and only then is the thermodynamic description appropriate. In some cases, such as electron transfer, reaction rates are predicted[2–5] and observed[6–8] to be controlled by the rate of solvent equilibration. But what is the rate of solvation in a given solvent? Although a key ingredient in understanding dynamical solvent effects on reactions, this is a question for which few systematic experimental studies are available.

In this work we focus on measuring the dynamics of solvation using picosecond time-resolved fluorescence spectroscopy. Time-resolved extensions of well-known steady-state methods for studying solvation energetics[9] provide an experimental monitor of solvent motions about a probe solute. After short-pulse electronic excitation, the fluorescence spectrum of a probe solute red shifts in time as the surrounding solvent reequilibrates to the new, excited state charge distribution. This time-dependent fluorescence shift provides a direct measure of the kinetics of solvation occurring at the microscopic level of relevance to chemical reactions. Although the feasibility of measuring solvation dynamics in this manner was demonstrated over a decade ago,[10] only very recently have both the theoretical development and experimental time resolution been sufficient to yield useful results.

Theoretical studies have nearly all approached the problem of solvation dynamics with a continuum treatment of the solvent. Since the earliest work of Bakshiev and Mazurenko,[11,12] an Onsager-type cavity solute interacting with a dielectric continuum has been used to model time-dependent spectral shifts. More recent theories have extended the description to include probe rotation[13] and "polarization diffusion"[14] effects, as well as a description of how the spectral shape changes with time.[15] Roughly speaking, these theories all predict that solvation, as measured by the fluorescence spectral shift of a probe solute, should proceed exponentially

 0021-9606/87/116221-19$02.10

in time with a time constant equal to the solvent's longitudinal relaxation time τ_L. This longitudinal response time is a bulk property of the solvent and is much faster than solvent reorientation times in polar liquids.

Experimental results to date have seemed to at least superficially corroborate the predictions of these continuum-based theories. For example, in our own recent study with the probe LDS-750,[16] solvation times in a number of polar aprotic and alcohol solvents were found to be approximately equal to the τ_L predictions. Some suggestions of important "molecular" contributions were found but the presently available data is too scarce to provide an adequate test of theories of solvation dynamics. More results with a variety of probe/solvent combinations are required.

In the present work we have continued our studies of solvation dynamics, here using the time-correlated single photon counting technique and the probe solute coumarin 153 (hereafter Cu153).

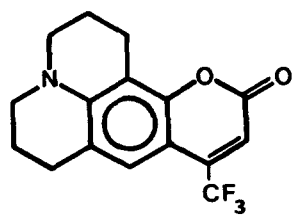

Coumarin 153

This probe was chosen because it is a rigid molecule having a single low-lying excited state and simple solvatochromatic behavior.[17–19] We have measured solvation dynamics in a variety of solvents including alcohols, an amide, and the polar aprotic solvent propylene carbonate, all as a function of temperature. We find that the observed dynamics are *not* accounted for on the basis of continuum descriptions of solvation. Molecular aspects of the solvent–solute interaction cause the detailed time dependence as well as the overall time scale of solvation to deviate from their predicted behavior. We believe that the deviations observed with Cu153 are a general phenomenon and not dependent on specific hydrogen bonding or other special interactions of this particular system. Rather this behavior results from a basic inadequacy of continuum models for describing molecular solvation.

The structure of this paper is as follows. In Sec. II we give a brief summary of the continuum theory predictions that we use to compare to our experimental results. Further details of the continuum theories are also discussed in the Appendix which reconciles an apparent difference between two theoretical treatments. After a brief experimental (Sec. III), Results (Sec. IV) are discussed in four subsections (A–D). We begin in Sec. IV A with results of semiempirical electronic structure calculations which provide insight into the S_0 and S_1 charge distributions of Cu153 that give rise to its solvatochromism. The solvent dependent shifts observed in steady-state spectra are then described in Sec. IV B. In Sec. IV C we discuss measurements of the rotational dynamics of Cu153. Since probe rotation can speed up the solvation rate, it is important to know how fast rotation is in relation to the solvent response. Rotational anisotropy measurements showed that in all cases studied here the normal rotation of Cu153 is too slow to noticably affect the observed solvation dynamics. In addition to the normal rotational behavior, an extra, unexpected anisotropy decay component was observed in this probe. We relate this component to a solvent-induced change in the electronic structure of the probe during solvation. Results of time-dependent spectral measurements are presented in Sec. IV D. Here we summarize the data relevant to solvation dynamics and compare our observed results to predictions of the continuum theories. Finally, in Sec. V we consider the present results obtained with Cu153 in relation to earlier studies of solvation dynamics. We attempt to show that the lack of agreement of our data with the predictions of continuum theory is a general problem reflecting the importance of molecular aspects of solvation. We conclude with a qualitative comparison of our results to some very recent work by Wolynes[20] on a molecular theory of solvation dynamics.

II. THEORETICAL

In order to provide a framework for discussing the experimental results we will briefly summarize some of the theoretical models used to describe time-dependent solvation. More detail on some aspects of the derivation of the equations presented here are given in the Appendix.

Most models of solvation treat the solvent as a continuum fluid which is fully characterized by its macroscopic dielectric properties. Adopting some simple model for the solute, these continuum approaches lead to predictions easily compared with spectroscopic measurements. A number of authors[21–23] have considered models in which the solute is a nonpolarizable point dipole centered in a spherical cavity. The change in the steady-state Stokes shift of the electronic spectrum upon going from the gas to polar solution is predicted to be

$$\Delta\bar{\nu}_a - \Delta\bar{\nu}_f = \frac{2(\mu_e - \mu_g)^2}{cha^3}\left[\frac{\epsilon_0 - 1}{2\epsilon_0 + 1} - \frac{n^2 - 1}{2n^2 + 1}\right]. \tag{1}$$

In this expression the $\bar{\nu}$ are the shifts (in cm^{-1}) of the absorption and fluorescence frequencies relative to their gas phase values. The solute parameters are the excited and ground state dipole moments μ_e and μ_g and cavity radius a. For simplicity, here and in the following discussion, we will assume μ_e and μ_g to be collinear. The solvent dependence is described by the reaction field functionality,

$$f(x) = \frac{x - 1}{2x + 1}, \tag{2}$$

in which x is the static dielectric constant ϵ_0 or the optical frequency dielectric constant, the refractive index (n) squared. The difference $f(\epsilon_0) - f(n^2)$ appears in Eq. (1), since it is assumed that the solvent fully equilibrates to the initial state of the electronic transition but only the optical frequency response of the medium is fast enough to follow the electronic transition itself. In order to be consistent with the time-dependent derivations to be described next, it is useful to generalize the above expression to include solute polarizability. In this case we have

$$\Delta\bar{\nu}_a - \Delta\bar{\nu}_f = \frac{2(\mu_e - \mu_g)^2}{chc a^3}\left(\frac{\epsilon_c + 2}{3}\right) \times\left[\frac{\epsilon_0 - 1}{2\epsilon_0 + \epsilon_c} - \frac{n^2 - 1}{2n^2 + \epsilon_c}\right], \quad (3)$$

where ϵ_c is the cavity dielectric constant, related to the solute polarizability α via the Clausius–Mossotti formula:

$$\frac{\alpha}{a^3} = \frac{\epsilon_c - 1}{\epsilon_c + 2}. \quad (4)$$

We assume that $\alpha(\epsilon_c)$ is the same in both electronic states. At this point it is worth noting that although many slight variations of the above equations have appeared in the literature,[24] the essential features are unchanged and Eq. (3) will be considered sufficient for our purposes.

The extension of the continuum solvent/polarizable point dipole solute model to describe the time-dependent fluorescence Stokes shift was carried out by Mazurenko,[12] Bagchi *et al.*,[13] and van der Zwann and Hynes.[14] Except for a minor error in the Bagchi formulation which is discussed in the Appendix, these analyses yield identical results. The time domain calculation requires a knowledge of the frequency dependent dielectric response of the solvent $\epsilon(\omega)$. In the simplest case, observed in many small, rigid molecules, $\epsilon(\omega)$ can be described by a single Debye dispersion as

$$\epsilon(\omega) = \epsilon_\infty + \frac{\epsilon_0 - \epsilon_\infty}{1 - i\omega\tau_D}, \quad (5)$$

where ϵ_0 and ($\epsilon_\infty = n^2$) are the static and infinite frequency dielectric constants and τ_D is the Debye relaxation time. In this case, after delta-function excitation, the fluorescence spectrum is predicted to shift with time as

$$\Delta\bar{\nu}_f(t) = \frac{-2(\mu_e - \mu_g)^2}{chc a^3}\left(\frac{\epsilon_c + 2}{3}\right)\left\{\frac{\epsilon_\infty - 1}{3(2\epsilon_\infty + \epsilon_c)}\mathcal{H}(t) + \frac{(\epsilon_c + 2)(\epsilon_0 - \epsilon_\infty)\tau_F}{(2\epsilon_\infty + \epsilon_c)^2\tau_D} e^{-t/\tau_F}\right\}, \quad (6)$$

where $\mathcal{H}(t)$ is the Heaviside step function and

$$\tau_F = \left(\frac{2\epsilon_\infty + \epsilon_c}{2\epsilon_0 + \epsilon_c}\right)\tau_D. \quad (7)$$

The step function part of Eq. (6) is the instantaneous response due to electronic polarization. The second, exponentially decaying part is what is experimentally observable.

In comparing experimental observation with theoretical predictions it is useful to work with the normalized spectral shift correlation function $C(t)$ defined by

$$C(t) = \frac{\bar{\nu}_f(t) - \bar{\nu}_f(\infty)}{\bar{\nu}_f(0) - \bar{\nu}_f(\infty)}, \quad (8)$$

where $\bar{\nu}_f(t)$, $\bar{\nu}_f(\infty)$, and $\bar{\nu}_f(0)$ are the fluorescence frequencies at times t, ∞, and 0. Expressed in this way, the frequencies need not be referenced to their (usually unknown) gas phase values. Further, since the magnitude of the shift is normalized out, different solutes and solvents can be readily compared. For a single Debye dielectric relaxation we have the simple result that $C(t)$ decays exponentially with time constant τ_F. Typically $\epsilon_0 \gg \epsilon_\infty, \epsilon_c$ and, therefore, τ_F is approximately equal to the solvent longitudinal relaxation time $\tau_L = (\epsilon_\infty/\epsilon_0)\tau_D$. In highly polar solvents $\tau_L \ll \tau_D$ and the decrease in solvation time scale from the solvent Debye time is a manifestation of the cooperative nature of the solvation response.

Bagchi *et al.*[13] considered the change in the time dependent shift when the probe can rotate in addition to the solvent dynamics. If the probe's motion can be described as an isotropic rotational diffusion with diffusion constant D, the response can still be described by Eq. (6) with τ_F replaced by τ_F':

$$\tau_F' = \left(\frac{1}{\tau_F} + 2D\right)^{-1}. \quad (9)$$

Thus, probe rotation, in this case random diffusional motion independent of the solvation dynamics, speeds up the observed spectral shift. If there is a substantial change in the direction of the probe's dipole moment upon excitation, a forced rotation of the probe due to the misaligned solvent reaction field might also serve to speed up the response. This latter effect has not yet been analyzed.

The majority of solvents have more complex dielectric responses than described by Eq. (5). Analytic solutions to the above continuum model can be made in a few instances. Particularly important is the multiple Debye form which is applicable to normal alcohols:

$$\epsilon(\omega) = \epsilon_{\infty n} + \sum_{j=1}^{n} \frac{\epsilon_{0j} - \epsilon_{\infty j}}{1 - i\omega\tau_{Dj}}. \quad (10)$$

If the regimes (j) are distinct such that for any ω,$\epsilon(\omega)$ is dominated by only one j then $C(t)$ decays as a sum of n exponentials:

$$C(t) = \sum_j a_j e^{-t/\tau_{Fj}} \quad (11)$$

with

$$\tau_{Fj} = \left(\frac{2\epsilon_{\infty j} + \epsilon_c}{2\epsilon_{0j} + \epsilon_c}\right)\tau_{Dj}. \quad (12)$$

and relative amplitudes

$$a_j \propto \frac{(\epsilon_{0j} - \epsilon_{\infty j})}{(2\epsilon_{\infty j} + \epsilon_c)(2\epsilon_{0j} + \epsilon_c)}. \quad (13)$$

For only two dispersion regimes Bagchi *et al.* were able to obtain $C(t)$ with no restrictions on the degree of overlap. The decay is double exponential as above,

$$C(t) = a_1 e^{-t/\tau_{F1}} + a_2 e^{-t/\tau_{F2}} \quad (14)$$

but with time constants (including probe rotation):

$$\tau_{F1} = (S_+ + 2D)^{-1},$$
$$\tau_{F2} = (S_- + 2D)^{-1}, \quad (15)$$

where

$$S_\pm = \tfrac{1}{2}\{A \pm \sqrt{B^2 - 4B}\} \quad (16)$$

$$A = \frac{(\tau_{D1} + \tau_{D2})(2\epsilon_\infty + \epsilon_c) + 2(\epsilon_{01} - \epsilon_{\infty 2})\gamma}{\tau_{D1}\tau_{D2}(2\epsilon_{\infty 2} + \epsilon_c)}, \quad (17)$$

$$B = \frac{(2\epsilon_{01} + \epsilon_c)}{\tau_{D1}\tau_{D2}(2\epsilon_{\infty 2} + \epsilon_c)}, \quad (18)$$

and

$$\gamma = \frac{(\epsilon_{01} - \epsilon_{\infty 1})\tau_{D2} + (\epsilon_{02} - \epsilon_{\infty 2})\tau_{D1}}{(\epsilon_{01} - \epsilon_{\infty 2})}. \quad (19)$$

The amplitudes are

$$a_1 = \left(\frac{S_+S_-}{S_+ - S_-}\right)\left(\gamma - \frac{1}{S_+}\right),$$
$$a_2 = \left(\frac{S_+S_-}{S_+ - S_-}\right)\left(\frac{1}{S_-} - \gamma\right). \quad (20)$$

For $\tau_{D1} \gg \tau_{D2}$ these expressions ($D = 0$) reduce as they should, to Eqs. (12) and (13).

The continuum treatments of solvation described above provide a useful framework for understanding real solvent behavior. For our purpose the main result is that the solvation time scale should be approximately equal to the solvent longitudinal relaxation time. Molecular aspects of the solvation process, not included in the continuum models, may be expected to modify this prediction and we find strong indications of this in our results. Unfortunately, more molecularly based models have not yet been developed to the point where they may be quantitatively compared to experiment. We will thus reserve the necessarily qualitative discussion of possible molecular effects until after we have presented our results.

III. EXPERIMENTAL

Coumarin 153 was obtained from Eastman Kodak ("Laser Grade") and was used without further purification. No sign of impurities were detectable in the steady-state spectra or fluorescence decays. Most of the solvents used were "spectrophotometric grade" from Aldrich Chemical. Propylene carbonate (Aldrich) and *N*-methylpropionamide (Eastman Kodak) were reagent grade. These latter solvents showed slight impurity fluorescence at wavelengths below 500 nm; however, the levels were low enough so as to affect insignificantly the time resolved fluorescence measurements. All solvents were dried over type 3A molecular sieves prior to use.

Steady-state absorption and fluorescence spectra were recorded on Cary 219 and Perkin–Elmer MPF-4 spectrometers, respectively. Fluorescence spectra were corrected using a quantum counter up to 600 nm. At wavelengths longer than 600 nm a correction based on parabolic extrapolation of the shorter wavelength correction was employed. Temperature control (-50 to $+20$ °C; ± 1 °C) in the steady-state as well as the time-resolved fluorescence measurements was achieved by circulating fluid from a Neslab ULT-80DD regulated bath through a brass sample block. Fluorescence samples were deoxygenated by bubbling nitrogen through them prior to use.

Time-resolved emission data were collected using the time-correlated single photon counting technique. Our apparatus has been described in detail elsewhere.[25] All experiments were performed using 405 nm excitation obtained by frequency doubling 810 nm light obtained with LDS-821 dye (Exciton) as the gain medium.[26] The detector was an ITT F4129 microchannel plate PMT with an instrument response function 110 ps FWHM which after deconvolution provided an effective time resolution of ~30 ps. Spectrally resolved decays were measured with magic angle polarization and using an ISA Model H10 monochrometer operated with a bandpass of 16 nm (FWHM) bandpass. For the anisotropy measurements the wavelength was chosen near the maximum of the steady-state emission and a 60 nm bandpass was employed in order to minimize possible artifacts caused by the spectral shifts. A Glan–Thompson and film polarizer were used for the excitation and analyzer polarizers and an anisotropy measurement consisted of three decays collected at magic angle, parallel, and perpendicular relative polarizations. The fluorescence decays and anisotropies were analyzed by fitting to sums of exponentials using an iterative reconvolution procedure. The anisotropy analysis involved simultaneous fitting of the parallel and perpendicular decays in the manner described in Ref. 27.

Time-resolved spectra were generated from a set of decays taken at 10 nm intervals spanning the fluorescence spectrum (typically 15 decays). To deconvolve the instrument response from the decay data, each decay was fit to a sum of exponentials. Three components were generally required to obtain a satisfactory fit to the data. The purpose of these fits is simply to represent the decay curves and no physical meaning is ascribed to the derived exponential parameters. The spectrum at a given time t, $S(\lambda;t)$, was obtained from the fitted decay series $D(t;\lambda)$ by relative normalization of different wavelengths using the steady-state fluorescence spectrum $S_0(\lambda)$ as

$$S(\lambda;t) = D(t;\lambda)\frac{S_0(\lambda)}{\int_0^\infty D(t;\lambda)dt}. \quad (21)$$

The steady-state spectra used for normalization were recorded at 1–3 nm resolution and then convoluted with a 16 nm FWHM Gaussian function in order to match the resolution used in obtaining the decays. A description of the method used to derive the spectral shift correlation function $C(t)$ from these spectra, $S(\lambda;t)$, is provided in Sec. IV D.

IV. RESULTS

A. MNDO calculations

The solvatochromic behavior of a probe solute depends on its dipole moments (charge distributions) in the S_0 and S_1 states. Since not even the ground state dipole moment of Cu153 or related compounds have been measured, it is of use to turn to electronic structure calculations to provide insight into what to expect of this probe molecule.[28] We have therefore performed semiempirical quantum mechanical calculations using the AMPAC computer program developed by Dewar and co-workers.[29] The calculations are based on the MNDO all-valence electron parametrization of the NNDO SCF approximation.[30] This method is known to yield reliable values for many ground state properties for molecules such as Cu153.[31–33] As an example, we calculate a ground state dipole moment of 4.58 D for Coumarin which compares well with the experimental value of 4.62 D.[34] Less reliability can be expected for excited state properties since the parametrization of this approach is based on ground state data. However, the excited state calculations do provide a semiquantative indication of the charge shifts expected between S_0 and S_1.

For the ground state S_0 a restricted Hartree–Fock calcu-

TABLE I. Properties of Cu153 obtained from MNDO calculations.

	S_0	S_1	$S_1 - S_0$
ΔH_f(kcal/mol)[a]	−191.4	−103.7	87.7
μ(D)	5.63	9.51	3.90
θ(deg)[b]	12	16	21

[a] Heat of formation relative to elements in their standard states.
[b] Orientation of the dipole moment measured as the angle between the coumarin 2–3 and 6–7 bond bisectors and μ as shown in Fig. 1.

lation with no configuration interaction was performed. The S_1 state was calculated including configuration interaction among the three singlet microstates formed from one and two electron excitations from the HOMO to the LUMO of the ground state wave function. In both cases all atoms within the ring system as well as all directly attached atoms were constrained to be planar. Further, the 2 alkyl rings holding the amino group rigid were assumed to be symmetric with respect to inversion about the nitrogen, and the 12 hydrogens in these rings were assumed to have equivalent bond lengths and HCC angles. All remaining degrees of freedom were optimized during the calculations.

A summary of properties calculated for the S_0 and S_1 states of Cu153 are given in Table I and atomic charge distributions are shown in Fig. 1. The most reliable results are for the ground state properties. A large dipole moment of 5.6 D is calculated for S_0 indicating that Cu153 should be strongly solvated in the ground state. The dipole moment lies approximately in the direction connecting the three and seven ring positions (Fig. 1) with the positive end toward the amino

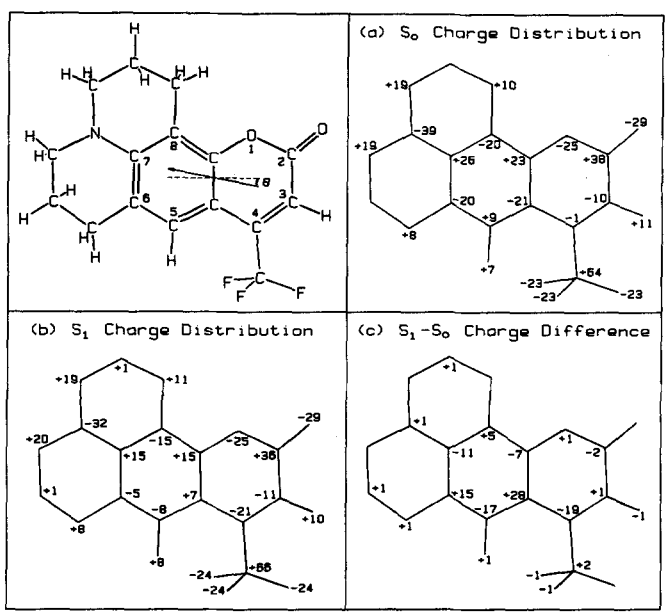

FIG. 1. Charge distributions calculated for Cu153. The first panel shows the atom numbering and the (S_0) dipole moment direction. The angle θ is defined relative to the bisector of the bonds between atoms 2,3 and 6,7. Panels (a)–(c) show the net atomic charges calculated for the ground state (a), the first excited state (b), and the S_1-S_0 difference charge distributions. Charges are given in units of percentage of an electronic charge. The charges shown at the CH_2 group positions are the sum of the charges for all three atoms.

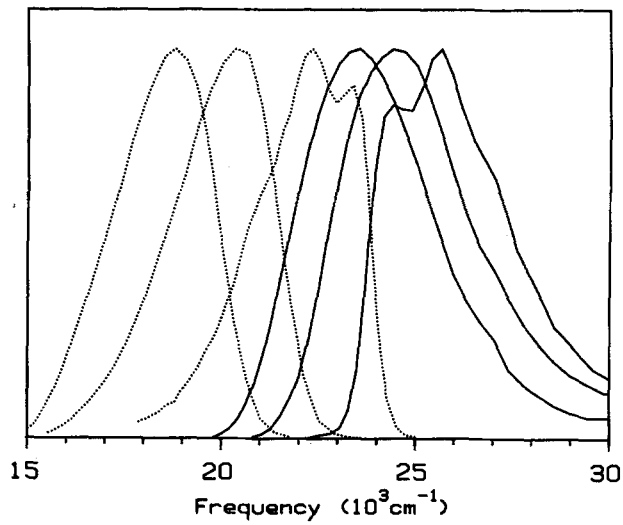

FIG. 2. Steady-state absorption (solid curves) and emission spectra (dotted curves) of Cu153 in three solvents. The solvents are *n*-hexane, *n*-butyl acetate, and dimethylsulfoxide in order of decreasing peak frequency.

functionality. Net atomic charges calculated for S_0 [Fig. 1(a)] show that the most polar solvent-accessible groups are all negatively charged; there are no particularly acidic hydrogens present. Thus, Cu153 is expected to have little hydrogen bond donating abilities but to be a good H-bond acceptor in the ground state. Both the carbonyl O and the amine N are good H-bond acceptors with the former probably being the less sterically hindered.

The S_1 excited state is calculated to lie 87.7 kcal/mol = 30 700 cm^{-1} higher in energy than the ground state. This value is ~22% higher than the experimental gas phase S_1--S_0 origin of 25 196 cm^{-1}.[36] The dipole moment is calculated to increase to 9.5 D while remaining in virtually the same direction as in S_0. The S_1--S_0 change of $\Delta\mu = 3.9$ D appears to come about mainly through charge redistribution within the coumarin ring system [Fig. 1(b)]. Electron donation from the amino group to the rings is quite small as are the changes on all pendant groups. Based on these calculations then, the solvation of the S_1 state of Cu153 should be qualitatively similar to but larger than solvation of the ground state. The change in hydrogen bonding strength is predicted to be small.

B. Steady-state spectra

Typical absorption and fluorescence spectra of Cu153 in three solvents of varied polarity (hexane, *n*-butylacetate, and DMSO) are shown in Fig. 2. The spectra in nonpolar solvents such as hexane exhibit some vibronic structure with a progression in a 1000 cm^{-1} mode. In more polar solvents this structure is quickly lost and fairly featureless spectra exemplified by that in DMSO are observed. The band positions and half-widths vary in a systematic way as a function of solvent polarity.

A summary of the steady-state absorption and emission data in a range of solvents is provided in Table II and Fig. 3. To measure solvent polarities we use the empirical π^* scale propounded by Kamlet *et al.*[37] We prefer this scale to other scales such as the E_T [Eq. (30)] scale[38] since it is based on

TABLE II. Steady-state spectral data (20 °C).

No.	Solvent	Solvent[a] polarity π^*	$f(\epsilon_0)-f(n^2)$[b]	Absorption λ_{max} (nm)	Absorption $\bar{\nu}$[c] (10^3 cm^{-1})	Absorption FWHM (10^3 cm^{-1})	Fluorescence λ_{max} (nm)	Fluorescence $\bar{\nu}$[c] (10^3 cm^{-1})	Fluorescence FWHM (10^3 cm^{-1})
1	*n*-hexane	−0.08	~0	390	25.67	3.77	448	22.23	3.29
2	cyclohexane	0.05	~0	395	25.49	3.75	452	22.12	3.16
3	triethylamine	0.14	0.048	396	25.33	3.83	466	21.42	3.24
4	diethylether[d]	0.27	0.167	(405)	24.95	···	(475)	20.82	···
5	*n*-butylacetate	0.46	0.171	409	24.67	3.99	490	20.03	3.08
6	tetrahydrofuran[d]	0.58	0.207	(413)	24.45	···	(500)	19.72	···
7	acetone[d]	0.72	0.284	(416)	24.25	···	(515)	19.12	···
8	propylene carbonate	0.81	0.286	421	23.95	4.04	522	18.76	3.08
9	dimethylformamide	0.88	0.274	422	23.92	4.04	524	18.74	3.06
10	dimethylsulfoxide	1.00	0.264	426	23.72	4.05	532	18.49	3.03
11	acetonitrile[d]	0.85	0.305	(418)	24.15	···	(522)	18.92	···
12	*t*-butanol[d]	1.41	0.251	(416)	24.25	···	(513)	19.22	···
13	2-propanol	0.46	0.273	420	24.08	4.06	520	18.85	3.01
14	*n*-butanol	0.46	0.263	421	24.03	4.01	525	18.74	2.99
15	*n*-propanol	0.51	0.274	422	24.03	4.10	528	18.64	2.94
16	ethanol	0.54	0.289	421	24.03	4.10	530	18.56	3.04
17	methanol	0.60	0.308	422	23.99	4.17	536	18.33	2.95
18	trifluoroethanol	0.73	~.32	438	23.15	4.20	538	18.22	2.91
19	*N*-methylpropionamide	···	0.289	419	24.10	4.01	529	18.67	3.11

[a] Values from M. J. Kamlet, J. L. M. Abboud, and R. W. Taft, Prog. Phys. Org. Chem. **13**, 485 (1981).

[b] Values of the reaction field function [f defined in Eq. (2)] describing the solvent dependence of the Stokes shift [Eq. (1)]. ϵ_0 and $n = n_D^{20}$ are from A. J. Gordon and R. A. Ford, *The Chemist's Companion* (Wiley, New York, 1972).

[c] $\bar{\nu}$ is the average frequency defined by the average of the frequencies at the two half-maximum points. This is a more reproducible frequency measure than the peak maximum.

[d] Frequencies for these solvents were estimated using the λ_{max} values (in parentheses) from G. Jones II, W. R. Jackson, S. Kanoktanoporn, and A. M. Halpern, Opt. Commun. **33**, 315 (1980). $\bar{\nu}$ values were estimated by shifting the reported frequencies ν_{max} by the average deviation between ν_{max} and our observed $\bar{\nu}$ for six common solvents. These shifts were + 250 and − 280 cm^{-1} for absorption and fluorescence, respectively.

the solvatochromic behavior of a number of different probe solutes. This feature has enabled the systematic removal of hydrogen bonding effects from π^*. In the nonalcoholic solvents (×) there is a linear relationship between the band frequency and polarity in both the absorption and emission spectra (Fig. 3). The lines drawn on Fig. 3 are the least-squares fits:

$$\bar{\nu}_{abs} = 25.505 - 1.779\pi^* \ (10^3 \ \text{cm}^{-1}), \quad (22)$$

$$\bar{\nu}_{em} = 21.910 - 3.667\pi^* \ (10^3 \ \text{cm}^{-1}). \quad (23)$$

Alcohols (○) do not follow the same correlation as do the aprotic solvents. The hydrogen bond donating ability of the alcohols provides an additional solvation mechanism. As already discussed this probably involves bonding with the amino or more likely the carbonyl group of the probe. Figure 3 shows that the effect of hydrogen bonding is to produce an additional shift in both absorption and fluorescence that is approximately constant over the range of alcohols studied. In *n*-propanol the hydrogen bonding contribution accounts for roughly 40% of the total absorption and emission shifts relative to cyclohexane.

The frequency–polarity correlations shown in Fig. 3 are as expected based on the calculated charge distributions in S_0 and S_1. The shifts indicate that both S_0 and S_1 are strongly solvated in polar solvents with the interaction in S_1 being greater. The hydrogen bond strength in the S_1 state is also larger than in S_0, a feature not predicted from the calculations. An experimental estimate for the change in dipole moment between the two states may be made using the continuum theory expression, Eq. (1). In Fig. 4 we have plotted the difference in absorption and emission frequencies vs the predicted solvent dependence given by the term in brackets in Eq. (1). Assuming parallel S_0 and S_1 dipoles and a cavity radius (a) of 3.9 Å (based on the van der Waals volume of Cu153), the slope of this plot yields a value $\Delta\mu = 6.0$ D. This value is significantly larger than the $\Delta\mu = 3.9$ D obtained from the semiempirical calculations. Such a difference could be a result of the calculations underestimating the degree of charge separation in S_1. Since the H-bond strengthening in S_1 indicated by experiment is not correctly predicted by the MNDO results, this hypothesis is not unfounded. However, to bring the "experimental" estimate into agreement with the calculated value all that would be required is to use a 20% smaller value for the cavity radius in Eq. (1). Thus, it is probably best to view the MNDO calculations and the solvatochromic shifts as being in agreement and pointing to an excited state dipole moment of roughly 10 D for Cu153.

The widths of the steady-state spectra show interesting correlations with polarity [Fig. 3(c)]. As the polarity of the solvent decreases, the FWHM of the absorption and fluorescence bands become more similar. In the gas phase limit these two widths are nearly equal (~4000 cm^{-1} at 230 °C[36]). One means of rationalizing the effect of solvation on spectral widths is illustrated in Fig. 5. In this model we expect that solute molecules will be inhomogeneously distributed over a range of solvent environments and that this

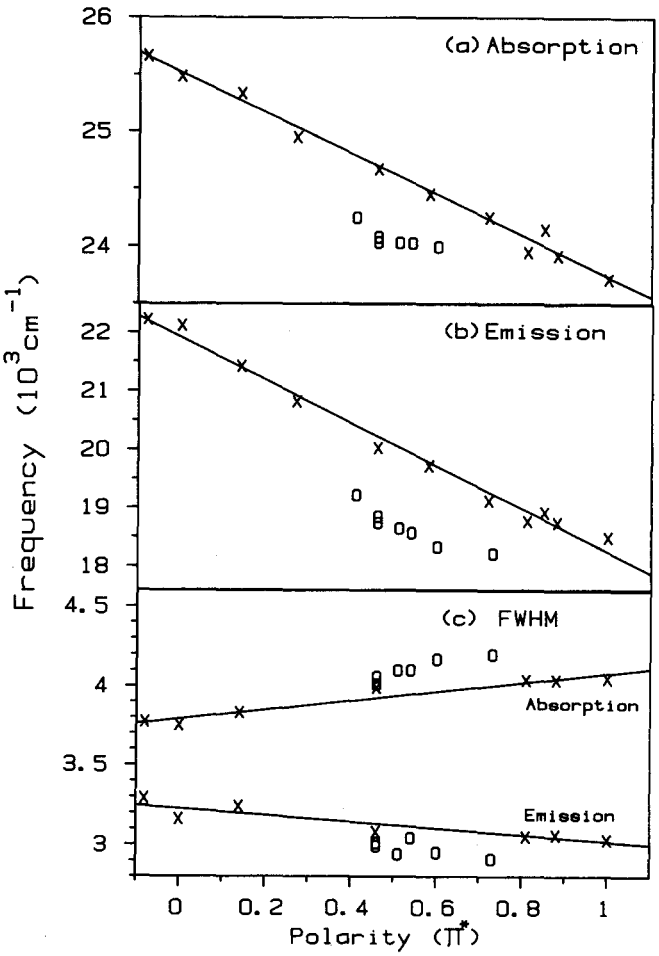

FIG. 3. Correlations of steady-state spectral properties with solvent polarity (π^*). (a) Average absorption frequency; (b) average emission frequency; and (c) absorption and emission bandwidths. (See Table II and the text for definitions of the average frequencies and π^*.) These data are for polar aprotic solvents (×) and alcohols (○). The lines drawn on the figures are least squares fits to the data excluding the alcohol points.

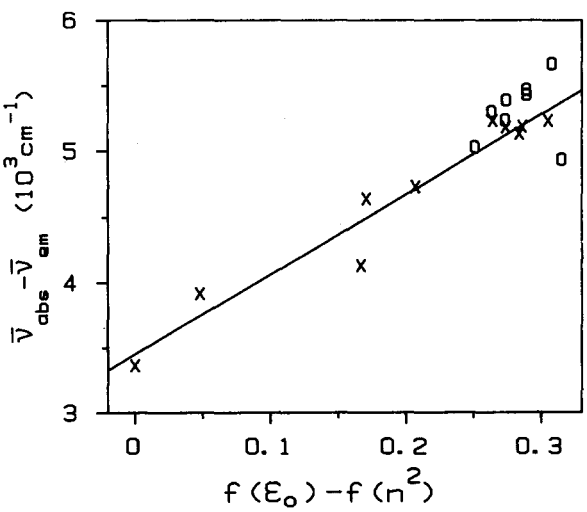

FIG. 4. Steady-state Stokes shifts (difference between average absorption and emission frequencies) plotted vs the reaction field function $f(\epsilon_0)$-$f(n^2)$ of Eqs. (1) and (2). These data are for polar aprotic solvents (×) and alcohols (○). The line is the least-squares fit to the polar aprotic solvent data. Based on a solute radius of a 3.9 Å and Eq. (1), the slope of this line indicates a change in solute dipole moment of 6.0 D.

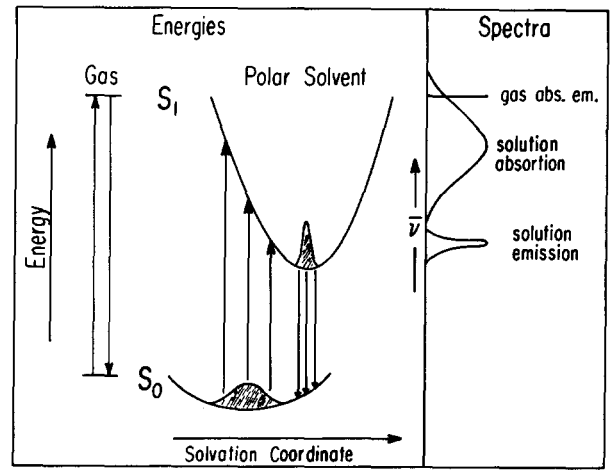

FIG. 5. Schematic diagram of solvation energies and their relation to the steady-state spectra. As indicated by the steady-state data for Cu153 we have drawn the S_1 state as being more strongly solvated than the S_0 state.

will lead to a broadening of the solution spectra relative to the purely intramolecular, Franck–Condon envelope observed in the gas phase. Since the solvation in S_1 is stronger than in S_0 we expect the curvature in the S_1 solvation potential well is probably also greater. As shown in Fig. 5 the broader distribution over solvent configuration in S_0 will lead to the solvation broadening in the absorption spectrum being greater than in the emission spectrum. The difference in the widths of the absorption vs fluorescence spectra should increase with increasing solvent polarity as is observed experimentally. There is a major problem with this picture however. The fluorescence spectra in solution are *narrower* than in the gas phase, and they *narrow* with increasing solvent polarity. To explain this behavior an additional solvent dependent mechanism must be invoked. One possibility is that the charge distribution of the S_1 state is itself slightly dependent on the strength of solvation. Changes in emission half-widths with polarity could then reflect small changes in Franck–Condon factors due to these electronic changes. The curious observation that the fluorescence spectrum of Cu153 in cyclohexane exhibits the most vibronic structure, even though it is broader than the featureless spectra seen in polar solvents (Fig. 2) is in line with this proposal. Further evidence will also be presented in the following sections.

C. Reorientational dynamics

In order to determine whether probe rotation could play a significant role in the observed Stokes shift dynamics, rotation times of Cu153 were measured in a number of solvents. The results obtained were rather unexpected. Multiexponential anisotropy decays, typified by the *n*-propanol data shown in Fig. 6, were observed. In Fig. 6(a) we have plotted the anisotropy decay $R(t)$ [Eq. (24)] obtained from tail-matched parallel $[I_{\parallel}(t)]$ and perpendicular $[I_{\perp}(t)]$ decays prior to deconvolution:

$$R(t) = \frac{I_{\parallel}(t) - I_{\perp}(t)}{I_{\parallel}(t) + 2I_{\perp}(t)}. \tag{24}$$

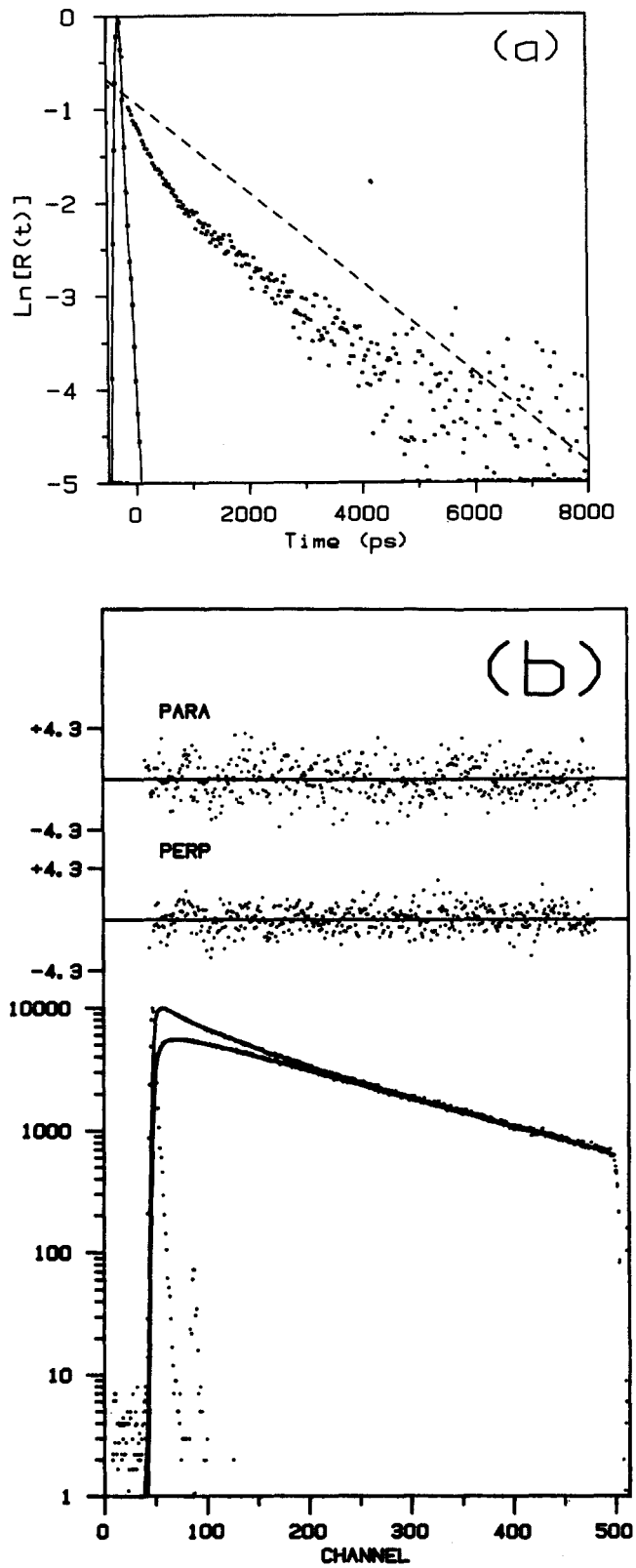

FIG. 6. Rotational anisotropy data for Cu153 in *n*-propanol (238 K). (a) Anisotropy decay $R(t)$ formed directly from the $I_{\parallel}$ and $I_{\perp}$ data as described by Eq. (24) without deconvolution of the instrument response. Data points are the $R(t)$ data. For comparison, the instrument response function (·-·-·) and the $R(t)$ expected from a hydrodynamic model (---; see the text) are also shown. (b) Example of simultaneous fitting of $I_{\parallel}(t)$ and $I_{\perp}(t)$ to obtain the deconvoluted $r(t)$ anistropy. $I_{\parallel}$ and $I_{\perp}$ decays are plotted together on the bottom panel along with an instrument response curve. At the top, the weighted residuals of $I_{\parallel}$ and $I_{\perp}$ are plotted. In this example $r(t) = 0.18 \exp(-t/2070\text{ ps}) + 0.16(-t/290\text{ ps})$.

The multiexponential nature of $R(t)$ is clear on this logarithmic scale. Figure 6(b) shows a simultaneous analysis of the parallel and perpendicular components in which $r(t)$, the deconvoluted anisotropy decay, was fit to a double exponential form:

$$r(t) = r_1 e^{-t/\tau_1} + r_2 e^{-t/\tau_2}. \tag{25}$$

In the example shown here $r_1 = 0.19$, $\tau_1 = 892$ ps and $r_2 = 0.14$, $\tau_2 = 128$ ps.

Based on hydrodynamic models, which work quite well for many similar dye molecules, one would anticipate the rotational anisotropy of Cu153 to decay approximately as a single exponential.[39] Using space-filling models we estimate the dimensions of Cu153 to be $11.2 \times 8.5 \times 4.0$ Å. The volume of a parallelapiped of these dimensions is 381 Å^3 and the van der Waals volume based on atomic increments[40] is 253 Å^3. The effective hydrodynamic volume should lie between these limits. Approximating the molecule as an oblate symmetric top with axial ratio of 0.4 and whose transition moment is perpendicular to the symmetry axis, hydrodynamic theory with stick boundary conditions would predict a biexponential $r(t)$ with decay constants $\tau_1 = 1.26\tau_D$ and $\tau_2 = 1.45\tau_D$, where $\tau_D = V\eta/kT$.[39] With only a 15% difference between τ_1 and τ_2, the biexponentiality would not be detectable with our experiment and only a single exponential decay with average time constant $\langle\tau\rangle \sim \frac{1}{4}\tau_1 + \frac{3}{4}\tau_2 = 1.40\tau_D$ could be observed. Thus, the observation of clear multiexponential behavior in $r(t)$, with two quite different time constants, is unexpected.

Fluorescence lifetimes and rotational anisotropy decay parameters are listed in Table III, and rotation times are plotted as a function of viscosity in Fig. 7. Before discussing the rotation data it is useful to consider the nature of the overall fluorescence decay in these systems. At times much longer than the spectral shift times all fluorescence decays are single exponential. In the solvents and temperatures examined the lifetimes varied by only ~25%, although there does appear to be a trend toward shorter τ_{fl} with increasing polarity/hydrogen bond strength in the alcohols. At earlier times, where anisotropies must be measured, the fluorescence decays are multiexponential due to the shifting of the spectrum. This is true even when collecting fluorescence over a fairly large spectral window. As a result, the anisotropy decay parameters may be subject to relatively large uncertainties. An indication of the expected accuracy of these data can be obtained by comparing the anisotropy decay fits for *n*-propanol data (253 K) recorded at different observation wavelengths. These data are listed at the bottom of Table III. The emission decays at the various wavelengths differ dramatically. For example, at 480 nm 95% of the fluorescence intensity decays with a time constant of ~200 ps whereas at 600 nm 50% of the intensity appears with a *rise time* of ~200 ps. It is encouraging that the parameters of the longer anisotropy component (r_1,τ_1) are consistent to ± 10%–15%. The parameters of the shorter component (r_2,τ_2) are much more uncertain and in this example vary by ± 30%–40%. We take the above variations as estimates for the uncertainties in the data of Table III.

In all of the solvents studied, the longer of the anisotro-

TABLE III. Fluorescence lifetime and anisotropy decay data.

Solvent	T (K)	Viscosity[a] (cP)	τ_{fl}[b] (ns)	Anisotropy decay parameters[c] $r(0)$	r_1	r_2	τ_1 (ps)	τ_2 (ps)
Ethanol	295	1.13	4.68	(0.21)	0.21	···	98	···
	253	2.76	4.60	0.30	0.18	0.12	370	94
n-Propanol	295	2.23	4.97	(0.23)	0.23	···	180	···
	252	6.18	4.71	0.34	0.19	0.14	900	130
	238	9.98	4.87	0.34	0.18	0.16	2000	280
	220	20.8	4.70	0.33	0.21	0.12	3000	300
n-Butanol	295	2.74	5.05	(0.23)	0.23	···	250	···
	252	10.4	4.80	0.32	0.20	0.13	1360	190
2-Propanol	296	2.28	5.24	(0.25)	0.25	···	160	···
	252	10.1	5.00	0.31	0.18	0.13	1030	190
N-methyl-	294	5.9	5.04	0.34	0.26	0.08	330	40
propionamide	252	23	5.12	0.36	0.27	0.09	2600	200
Propylene	296	2.56	···	0.31	0.31	···	150	···
Carbonate	252	9.65	5.59	0.35	0.35	···	760	···
	232	24.2	5.83	0.35	0.35	···	3100	···
		λ_{obs} (nm)[d]						
n-Propanol		518 ± 28	4.71	0.34	0.19	0.14	900	130
(253 K)		480 ± 8	4.53	0.37	0.20	0.17	760	70
		530 ± 8	4.71	0.33	0.19	0.14	1000	160
		600 ± 8	4.73	0.44	0.21	0.24	990	100

[a] Viscosity values interpolated from literature data. For the alcohols the compilations in Landolt–Bornstein 6 II/5a were used. Literature data for propylene carbonate and *N*-methylpropionamide were taken from J. Barthel, H. J. Gores, P. Carlier, F. Feuerlein, and M. Utz, Rev. Bunsenges. Phys. Chem. **87**, 436 (1983), R. Gopal and S. A. Rizvi, J. Ind. Chem. Soc. **43**, 179 (1966), respectively.

[b] Fluorescence lifetimes, ± 10%.

[c] Anisotropy decay parameters [Eq. (25)] obtained from single or double exponential fits to $I_{\parallel}, I_{\perp}$ data. $r(0) = r_1 + r_2$ is the $t = 0$ anisotropy whose limiting value is 0.4. $r(0)$ values in parentheses indicate cases where it is clear that the value is too small due to an unresolvably fast decay component.

[d] Decay parameters for *n*-proponal (253 K) observed at several emission wavelengths. ± values indicate FWHM of the emission bandpass used.

py components (r_1,τ_1) correlates sensibly with solvent viscosity (Fig. 7). The least-squares fit line drawn in Fig. 7 yields a molecular volume of 300 Å^3 (stick boundary conditions), which lies between the two volume estimates given earlier. Thus, this component may be ascribed to normal diffusional rotation.

In most cases a second anisotropy component (r_2,τ_2) was required to achieve reasonable fits to the data. The time constants for this second component are roughly an order of magnitude shorter than the first component and are much too fast to correspond to any diffusive rotational motion of the molecule. This is true irrespective of the assumed symmetry of the molecule or boundary conditions chosen. The effect of this faster component on the anisotropy decay is not small as may be judged by comparing the relative magnitudes of the amplitudes r_1 and r_2. For parallel absorption and emission dipoles the anisotropy at time zero has an amplitude $r(0) = 2/5$. The longer anisotropy component r_1 only accounts for half of the expected $r(0)$ in the alcohols ($r_1 \sim 0.2$). In *N*-methylpropionamide (NMP) and propylene carbonate (PC) the r_1 values are higher but still significantly below 0.4. If we think of the fast process as producing an average change in transition moment direction, the angles calculated from r_1 are $\Delta\theta \sim 19°$ for PC, $\Delta\theta \sim 28°$ for NMP, and $\Delta\theta \sim 35°$ in the alcohols.

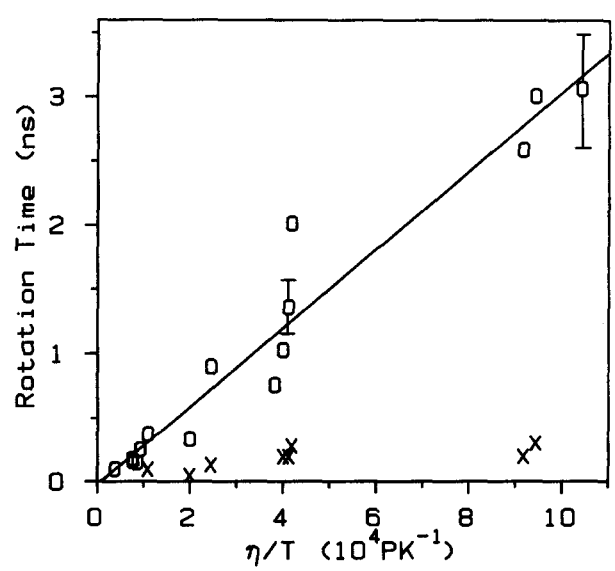

FIG. 7. Anisotropy decay times plotted vs viscosity (η/T). O's correspond to the longer (τ_1) of the two components for cases in which $r(t)$ was fit to a double exponential. In these cases the shorter component (τ_2) is plotted with an ×. The solid line is the least-squares fit to the τ_1 data. Is slope corresponds to a molecular volume of 300 Å^3 assuming stick boundary conditions (see the text).

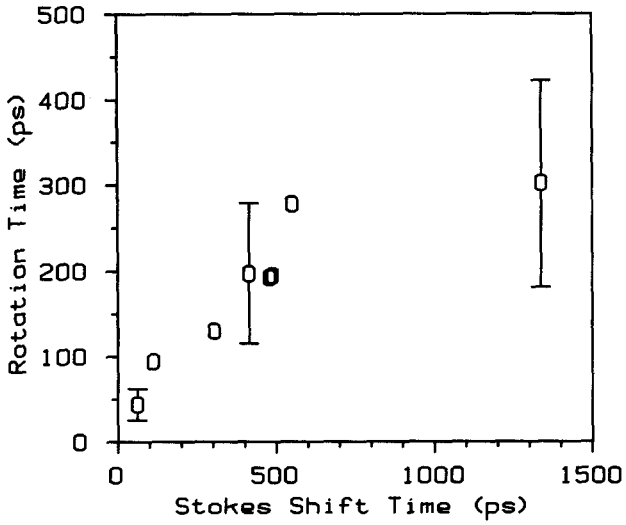

FIG. 8. Correlation of the fast rotational component (τ_2) to the Stokes shift (solvation) times. The latter times correspond to that of Table VI and are defined in the text of Sec. IV D.

It is interesting to speculate on the mechanism of this fast component of the anisotropy decay. The observed τ_2 time constants are roughly correlated with η/T as shown in Fig. 7, however a better correlation is obtained between τ_2 and the solvation times τ_{sol} measured via Stokes shift measurements (Fig. 8). The method by which τ_{sol} is obtained will be described in detail in the following section, here it is sufficient to note that the fast rotational component appears to be somehow related to the solvation dynamics. From Fig. 8 it appears that $\tau_2 \sim \frac{1}{3}\tau_{sol}$. We note that $\tau_2 \neq \tau_{sol}$ does not invalidate the causal relationship between this fast anisotropy decay component and solvation dynamics. The fluorescence anisotropy decay experiment measures the $l=2$ Legendre polynomial correlation function P_2:

$$r(t) = \tfrac{2}{5}\langle P_2\{\cos[\Delta\theta(t)]\}\rangle = \tfrac{2}{5}\langle \tfrac{3}{2}\cos^2[\Delta\theta(t)] - \tfrac{1}{2}\rangle \quad (26)$$

of the change in transition moment direction $\Delta\theta(t)$. If $\Delta\theta(t)$ decayed with the solvation time constant τ_{sol} we would, in general, expect $P_2[\Delta\theta(t)]$ to decay faster. For example, for a diffusive rotation in which $P_1 = \cos[\Delta\theta(t)]$ decays with time constant τ, the P_2 correlation function decays with time constant $\frac{1}{3}\tau$. Thus, the observation $\tau_2 \sim \frac{1}{3}\tau_{sol}$ is not surprising. The fast rotational component is not an artifact of the method of obtaining anisotropies but rather reflects a real physical process. Two possibilities seem plausible at present. The first is that there is a substantial change in the dipole direction between S_0 and S_1. Then, immediately after absorption, the misaligned reaction field of the Franck–Condon solvent state produces an instantaneous torque on the S_1 dipole that causes a forced rotation of the solute. Such forced motion could be considerably faster than diffusive rotation and account for the fast component. Although our MNDO calculations do not indicate much change in dipole direction, this mechanism cannot be ruled out on this basis alone. An alternative explanation is that there is no physical rotation of the probe at all but rather only a rotation of the transition moment. That is, due to solvent perturbations (nonspecific solvation, hydrogen bonding, etc.) the electronic charge in S_1 redistributes slightly to accommodate the S_1 solvent environment thus causing a rotation of the transition moment. This latter mechanism is in keeping with there being a change in electron distribution in S_1 as a function of the state of solvation, as previously inferred from the steady-state spectra. Either of the two mechanisms seems possible, however, and further anisotropy measurements are needed to help interpret this surprising behavior. For the present, these observations warn that a picture of the probe molecule as a passive observer of the solvation process may be too simplistic.

D. Stokes shift dynamics

This section is divided into two parts. Characterization of the time-dependent solvation response of a particular solvent entails obtaining the spectral shift correlation function $C(t)$ defined by Eq. (8). The method used to obtain $C(t)$ from the experimental data is somewhat involved and is described in the first part. Here we also discuss parametrization of the observed $C(t)$ functions and the uncertainties in the results. The second subsection then discusses the general features of the observed $C(t)$ correlation functions and relates these results to behavior expected based on continuum models of solvation.

1. Method of analysis

An example of a typical time-evolving spectral series is shown in Fig. 9. From such spectra we wish to extract the Stokes shift correlation function $C(t)$ of Eq. (8). As a first step we must define some characteristic frequency $\nu(t)$ of the spectrum with which to measure the spectral shift. The choice is complicated by the fact that the band shape, as well as its frequency, changes with time. To make full use of the data, we determine frequencies by first fitting the spectral points to a log-normal line shape function $g(\nu)$ defined by[41]

$$g(\nu) = \begin{cases} g_0 \exp\left\{-\ln(2)\left(\dfrac{\ln[1+2b(\nu-\nu_p)/\Delta]}{b}\right)^2\right\} \\ \qquad \alpha > 1 \\ 0, \quad \alpha \leqslant 1 \end{cases}$$
$$\alpha = 2b(\nu-\nu_p)/\Delta. \quad (27)$$

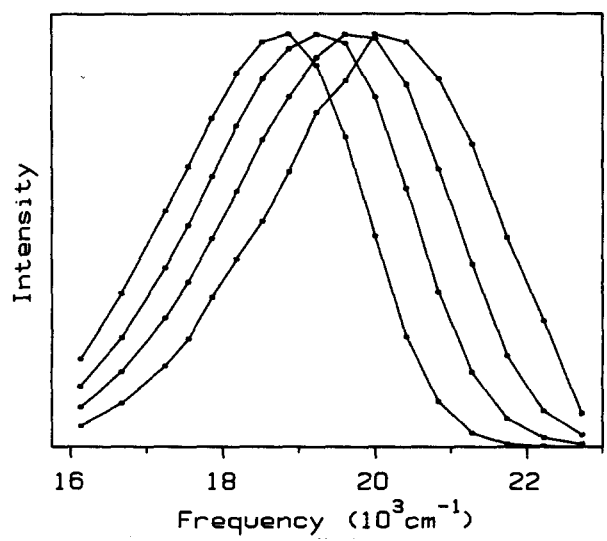

FIG. 9. Time-evolving fluorescence spectra of Cu153 in *N*-methylpropionamide (245 K). The times are 0, 100, 500, and 5000 ps after excitation in order of decreasing peak frequency.

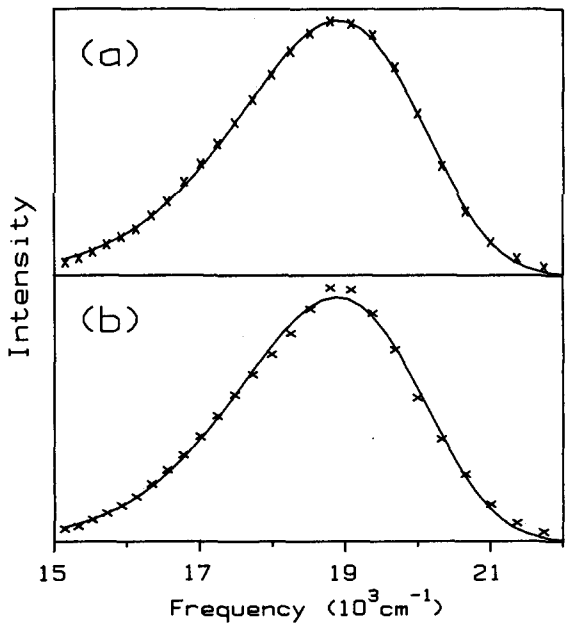

FIG. 10. Steady-state emission spectra of Cu153 fit to log normal line shapes. (a) *N*-methylpropionamide (245 K) and (b) *n*-propanol (222 K) represent the best and worst case fits (solid curves) to Cu153 spectra (×).

This four-parameter function describes an asymmetric line shape which reduces to a Gaussian function in the limit $b = 0$. The parameters g_0, ν_p, and b are the peak height, peak frequency, and asymmetry parameter, respectively. The FWHM, Γ, of this function is related to the width parameter Δ by

$$\Gamma = \Delta\left(\frac{\sinh(b)}{b}\right). \tag{28}$$

The ability of the log normal to represent spectra of Cu153 is illustrated by fits to the steady-state data shown in Fig. 10. Even though the observed spectrum contains a slight shoulder in some polar solvents [Fig. 10(b)], the fit is still good.

Once the spectra have been fit the data are then represented by the fitting parameters as a function of time, i.e., $g_0(t)$, $b(t)$, $\nu_p(t)$, and $\Delta(t)$. In general, we observe that the peak frequency $[\nu_p(t)]$ decreases, the width $[\Delta(t)]$ decreases, and the asymmetry $[b(t)]$ increases with increasing time. Although the primary change is in the frequency shift, because of band shape changes, the $C(t)$ correlation function depends slightly on the manner in which $\nu(t)$ is chosen. This effect is illustrated in Fig. 11(a) which shows four possible methods of measuring $\nu(t)$ (see the caption). In this example the average time constants of the different $C(t)$ curves differ by up to 35%. With such variations in mind, we will hereafter use an average frequency $\bar{\nu}$ defined by

$$\bar{\nu} \equiv \frac{\int_{-\infty}^{\infty} g(\nu)\nu\, d\nu}{\int_{-\infty}^{\infty} g(\nu) d\nu} = \nu_p + \left(\frac{\Delta}{2b}\right)\left[\exp\left(\frac{3b^2}{4\ln(2)}\right) - 1\right]. \tag{29}$$

Since theoretical approaches have so far considered the dynamical Stokes shift in terms of average solvation energies, this first moment $\bar{\nu}(t)$ is probably the best choice for comparison.

Two methods were used to extract $C(t)$ information from the $\bar{\nu}(t)$ data. In the first method we simply assess time

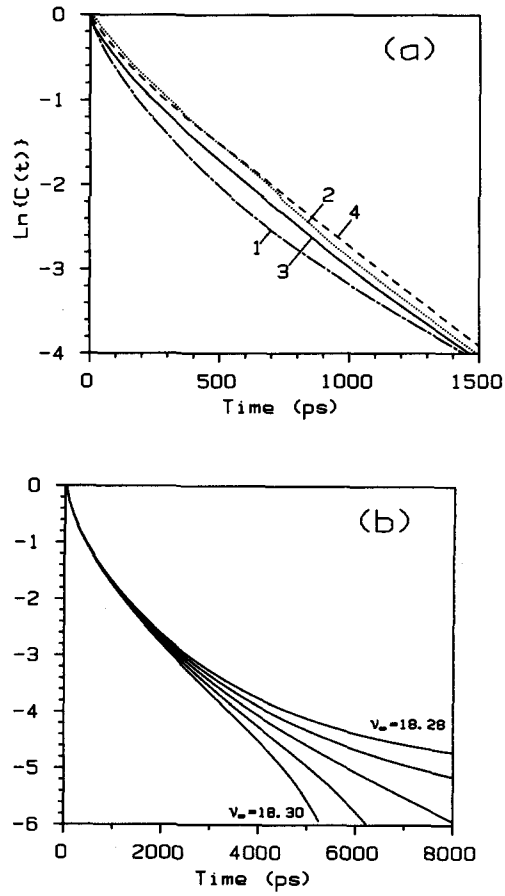

FIG. 11. Possible ambiguities in determining $C(t)$ from the time-resolved spectral data. (a) A series of $C(t)$ functions for the same *n*-propanol (253 K) data determined using the following choices for defining $\nu(t)$ from the spectrum: (1) the average of the half-height points; (2) the high-frequency half-height point; (3) the peak frequency of the fitted spectrum; (4) the average (first moment) frequency of the fitted spectrum. The average time constants [Eq. (30)] determined by these four choices are 280, 330, 230, and 320 ps, respectively. (b) A series of $C(t)$ curves obtained from the same $\nu(t)$ data with $\nu(0)$ fixed and with varying $\nu(\infty)$ choices. This data set is in *N*-methyl propionamide (244 K).

zero and time infinity values $\bar{\nu}(0)$, $\bar{\nu}(\infty)$ by inspection and form $C(t)$ directly as the ratio $C(t) = [\nu(t) - \bar{\nu}(\infty)]/[\bar{\nu}(0) - \bar{\nu}(\infty)]$. Extrapolation of the $\bar{\nu}(t)$ data to $t \to 0$ is relatively straightforward, however, there is some ambiguity in the choice of $\bar{\nu}(\infty)$. The long-time features of the $C(t)$ curves depend on changes of $\bar{\nu}(\infty)$ as small as $10 - 20$ cm^{-1}, which is only 0.5% of the width of the spectrum. The fitting procedure described above cannot accurately follow such minute changes and so $\bar{\nu}(\infty)$ must be judged based on "reasonable" limiting behavior of the $C(t)$ curves as a function of $\bar{\nu}(\infty)$. As an illustration, Fig. 11(b) shows a typical series of $C(t)$ curves generated from a single set of $\bar{\nu}(t)$ data with different $\bar{\nu}(\infty)$ values. [Note the larger dynamic range, 6*e*'s, in Fig. 11(b).] In this case we would choose the $\bar{\nu}(\infty)$ of the central curve as the best guess for the true $t = \infty$ value. Several $C(t)$ curves generated in this way are shown in Figs. 13 and 14, and parameters which characterize the $C(t)$ decays for all of the solvents studied are collected in Table IV. Since the decays are not single exponential functions, a number of different types of measured times are listed in the table.

TABLE IV. Characteristic time constants (ps) of the $C(t)$ decays.

Solvent	T (K)	t_{1e}[a]	t_{3e}[a]	S_{1e}^{-1}[b]	S_{3e}^{-1}[b]	$\langle\tau\rangle_{int}$
Ethanol	253	100	140	140	180	118
n-Propanol	295	49	69	77	82	56
	273	130	160	140	180	130
	251	290	380	380	430	320
	232	511	870	840	1100	690
	221	1100	2000	1900	2200	1300
n-Butanol	253	390	600	570	740	510
2-Propanol	253	460	640	630	910	530
N-methyl-	273	97	130	120	170	140
proponamide	244	440	780	640	1200	600
Propylene	252	47	47	47	50	47
Carbonate	237	76	110	100	170	86
	221	360	600	520	830	500

[a] Times t_{1e} (or t_{3e}) are defined such that $\ln[C(t)] = -1$ (or -3).

[b] Time constants defined by the slopes of the $\ln[C(t)]$ vs t plots at the times t_{1e} and t_{3e}: $S_{1e}^{-1} = (\partial \ln[C(t)]/\partial t)_{t_{1e}}^{-1}$.

[c] Average time constant [Eq. (30)] obtained for numerical integration of the $C(t)$ decays.

For comparison to predicted solvation time scales we will most often use the average time defined by

$$\langle\tau\rangle \equiv \int_0^\infty C(t)dt. \tag{30}$$

Values of $\langle\tau\rangle$ listed in Table IV were obtained by numerical integration of the $C(t)$ curves.

As a second means of characterizing the $C(t)$ decays, we fit the $\bar{\nu}(t)$ data to

$$\bar{\nu}(t) = \bar{\nu}(\infty) + [\bar{\nu}(0) - \bar{\nu}(\infty)]C(t) \tag{31}$$

with $C(t)$ analytically represented as either a sum of exponentials,

$$C(t) = a_1 e^{-t/\tau_1} + a_2 e^{-t/\tau_2} + \cdots \quad \sum_i a_i = 1 \tag{32}$$

or as a "stretched" exponential function[42]

$$C(t) = e^{-(t/\tau)^\alpha}. \tag{33}$$

As described in Sec. II, there is some justification for use of a multiexponential form for $C(t)$, at least in the alcohols. At present we have no such justification for the stretched exponential form, however, it does yield a good representation of the $C(t)$ data with fewer adjustable parameters than the multiexponential representation. Examples of typical fits are provided in Fig. 12 and the parameters are summarized in Table V. All fits were made using $\bar{\nu}(t)$ data within the time range $t = 10$ ps to $t = t_{4e}$, where $\ln[C(t_{4e})] = -4$ with $C(t)$ constructed as above. Both the multiexponential and stretched exponential fits may be used to regenerate the observed $\bar{\nu}(t)$ decays in this time range to within the estimated experimental uncertainty. Included with each fit is the average time constant $\langle\tau\rangle$ [Eq. (30)] calculated analytically from the fitted parameters.

We now discuss the experimental uncertainties in the determination of $C(t)$ curves. The smooth appearance of the results shown in Figs. 11–14 is a consequence of the two stages of fitting used in transforming the observed fluorescence decays into $\bar{\nu}(t)$ data, and is not a good gauge of experimental uncertainties. Better estimates of the probable accuracy can be obtained from repeated measurements and analysis of simulated data. For experiments with the same solvent and temperature that were performed many months apart we find good agreement of the derived $C(t)$ curves. Specifically, at times greater than 100 ps the $[\bar{\nu}(t) - \bar{\nu}(\infty)]$ values and the characteristic parameters of the $C(t)$ curves agree to within 10%. At earlier times (within our instrumental response function) the deviations are somewhat greater, up to 30%. From such comparisons we estimate that the average time constants $\langle\tau\rangle$ reported here are reproducible to within $\pm$ 10% for $\langle\tau\rangle \geqslant 200$ ps and $\pm$ 20% for smaller $\langle\tau\rangle$. The accuracy of our method of extracting $C(t)$ from the measured decays can also be examined with the aid of simulated data. Beginning with an assumed $C(t)$ function (chosen as mono or biexponential) and spectral parameters similar to those of the real spectra we constructed a set of simulated fluorescence decay data $[D(t;\lambda)$ in Eq. (21)]. Each decay was given a random time-zero shift, convoluted with an experimental instrument response function, and given noise appropriate to photon counting statistics so as to mimic real fluorescence data. Simulated data sets were then subjected to the same analysis used for the real data and the derived $C(t)$ parameters compared to those input. The results of such tests showed that the method of analysis accurately reproduced the input $C(t)$ behavior. For input average time constants greater than 100 ps, $\langle\tau\rangle$ was reproduced to better than 5%. Further, the shapes of the $C(t)$ curves were well reproduced except at very early times (30 ps). For example, if the input $C(t)$ was monoexponential, the resultant $C(t)$ was also clearly single exponential over at least four lifetimes. Thus, the highly nonexponential decays observed experimentally are not an artifact of the analysis. Fast components in the $C(t)$ decays (< 50 ps) could also be ex-

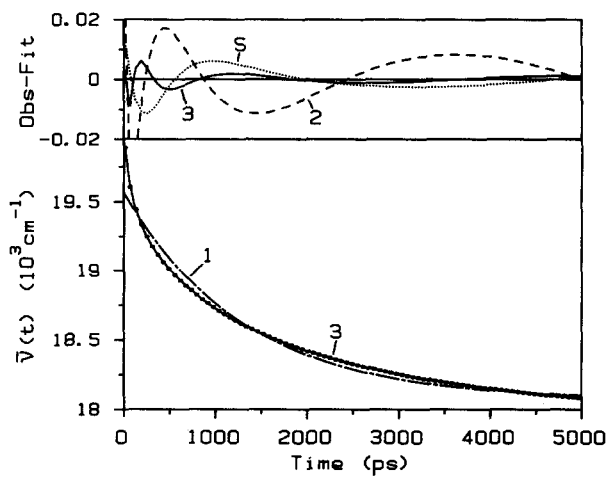

FIG. 12. Fits to $\bar{\nu}(t)$ data in *n*-propanol (222 K). The symbols 1,2,3, and *S* correspond to fits to single, double, and triple exponential, and stretched exponential functions, respectively. The bottom panel shows the $\bar{\nu}(t)$ data along with fitted curves for single and triple exponential fits. The top panel shows the residuals for all but the single exponential fit. In this example single and double exponential functions were judged inadequate to accurately represent the $\bar{\nu}(t)$ data.

TABLE V. Parametrization of the $\bar{\nu}(t)$, $C(t)$ data obtained from analytical fits.

		Sum-of-exponentials fit[a]						Stretched exponential fit[b]				
Solvent	T (K)	$\bar{\nu}_\infty$	$(\bar{\nu}_0-\bar{\nu}_\infty)$	$\tau_1(a_1)$	$\tau_2(a_2)$	$\tau_3(a_3)$	$\langle\tau\rangle$[c]	$\bar{\nu}_\infty$	$(\bar{\nu}_0-\bar{\nu}_\infty)$	τ	α	$\langle\tau\rangle$
EtOH	253	18.120	1.504	150(0.695)	31.4(0.305)	···	114	18.097	1.622	96.1	0.723	118
n-PrOH	295	18.420	1.213	78.8(0.681)	9.3(0.319)	···	56.6	18.387	1.159	58.0	0.719	71.5
	273	18.248	1.397	245(0.387)	87.6(0.612)	···	149	18.272	1.431	121	0.858	131
	251	18.180	1.460	430(0.700)	101(0.300)	···	331	18.166	1.533	289	0.767	337
	232	18.061	1.966	1110(0.527)	254(0.259)	28.9(0.214)	658	18.000	1.999	561	0.595	853
	221	17.937	2.007	2560(0.508)	572(0.278)	86.3(0.214)	1480	17.813	2.227	1220	0.532	2200
n-BuOH	253	18.223	1.842	747(0.559)	189(0.308)	44.6(0.133)	481	18.199	1.937	386	0.664	515
2-PrOH	253	18.333	1.545	648(0.727)	103(0.273)	···	499	18.307	1.613	445	0.729	543
N-methyl-	273	18.4	1.3	165(0.554)	48.1(0.446)	···	113	18.424	1.215	112	0.877	120
propionamide	244	18.323	1.545	793(0.570)	154(0.429)	···	518	18.304	1.694	338	0.653	528
								18.369	0.627	47.2	1.00	47.2
Propylene	252	18.369	0.627	47.2(1.00)	···	···	47.2	18.333	0.795	76.6	0.767	89.5
Carbonate	237	18.343	0.807	105(0.732)	14.6(0.266)	···	80.6	18.252	1.060	335	0.656	453
	221	18.257	0.967	773(0.506)	161(0.494)	···	471					

[a] Parameters as described in Eqs. (31) and (32).
[b] Parameters as described in Eqs. (31) and (33).
[c] Average time constants Eq. (30) calculated analytically from the fitted functions. For the sum-of-exponentials fit $\langle\tau\rangle = \Sigma_i a_i\tau_i$ and for the stretched exponential fit $\langle\tau\rangle = (\tau/\alpha)\Gamma(1/\alpha)$, where Γ is the gamma function.

tracted from the $C(t)$ data albeit with a reduced accuracy ($\pm 20\%$). We estimate that our experimental results should give a reasonable account of all components in the $C(t)$ decays with time constants greater than 30 ps. Behavior at shorter times cannot be extracted from the present data.

One further aspect of the $C(t)$ data to consider is how our finite time resolution affects the comparison to predicted behavior. As pointed out by Nagarajan *et al.*,[43] a finite time-resolution experiment really measures a correlation function $C'(t)$ that differs from the true $C(t)$ to the extent that the apparent $\bar{\nu}(0)$ is in error due to limited time resolution. In the triacetin solutions studied, these authors found indications that the apparent $\bar{\nu}(0)$ obtained using methods similar to ours were substantially different than independent estimates of the true $t = 0$ value. One may ask if this is the case with the present data and, if so, how does it influence the reported results? Two observations argue against there being a large error in the apparent $\bar{\nu}(0)$ values. First, the peak frequencies at $t = 0$ are approximately what would be expected based on the steady-state absorption spectra. In a given solvent the fluorescence spectral origin at $t = 0$ should be equal to the origin of the steady-state absorption spectrum. We cannot assign band origins, however, we can compare peak frequencies in a solvent vs the gas phase peak frequencies. In the gas phase, where the band origins coincide, a shift of 3500 cm^{-1} (230 °C)[36] is observed between the absorption and emission maxima as a result of vibrational structure. In

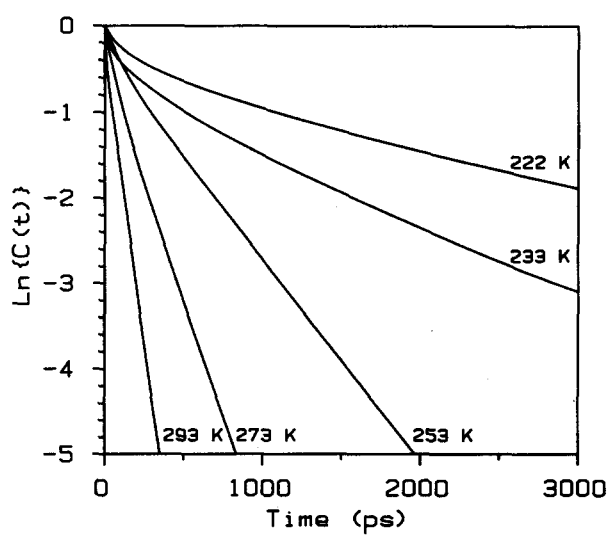

FIG. 13. $C(t)$ correlation functions observed in *n*-propanol at a series of temperatures.

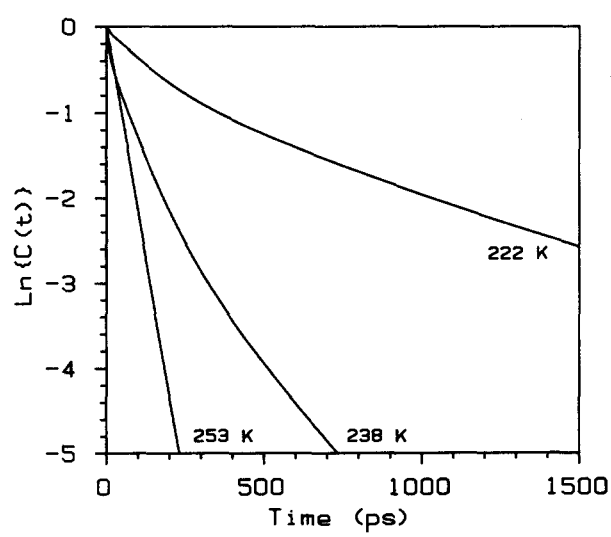

FIG. 14. $C(t)$ correlation functions observed in propylene carbonate at a series of temperatures.

solution the $t = 0$ fluorescence spectral maxima are also shifted from the steady-state absorption maxima by approximately this same amount. Based on such comparisons we estimate that we are observing more than 70% of the total $\bar{\nu}(0) - \bar{\nu}(\infty)$ shift in our time-dependent spectra. Second, the behavior of the $\bar{\nu}(0)$ and $\bar{\nu}(0) - \bar{\nu}(\infty)$ values (Table V) in a given solvent change predictably as a function of temperature. That is, as the temperature is lowered the magnitude of $\bar{\nu}(0) - \bar{\nu}(\infty)$ increases somewhat in a manner easily accounted for based on the changing solvent polarity. If we were missing a large portion of the shift at early times we would expect much more pronounced changes with temperature as the fast processes slowed down (probably exponentially) with decreasing temperature and moved within our experimental time resolution. Unless there is a fast component of $C(t)$ which throughout the temperature range studied remains faster than our time resolution, we should indeed be observing the true $C(t)$ decay. Finally, we note that even if there were unresolvable fast components causing the apparent $\bar{\nu}(0)$ to be too low, our findings would not be qualitatively affected. For example, plotted on a logarithmic scale as are Figs. 13–15, the difference between the true and apparent $C(t)$ is only a constant vertical shift. Since we are interested in solvents whose predicted $C(t)$ decays are single exponential over most of the experimental time window, a constant shift is of little consequence in comparing observation to theory. This is not the case for triacetin studied by Nagarajen *et al.*[43] because here the predicted $C(t)$ decays are highly nonexponential. Our $\langle\tau\rangle$ values will of course be too large if we have missed some short-time component in $C(t)$. However, we only compare $\langle\tau\rangle$ to the predicted long-time (exponential) behavior in these solvents, so that the observation of $\langle\tau\rangle$ greater than predicted is still a significant result.

2. C(t) results

Parameters characterizing the observed spectral shift correlation functions $C(t)$ are summarized in Tables IV and V. In Figs 13 and 14 we have plotted representative $C(t)$ decays observed in *n*-propanol and propylene carbonate as a function of temperature. One obvious feature of the data is that the observed correlation functions are not single exponential. As is clear from Figs. 13 and 14 and the $C(t)$ fits in Table V, the $C(t)$ curves indicate the presence of multiple relaxation times, or a continuous distribution of relaxation times in the solvation process. Such $C(t)$ functions are not consistent with continuum-model predictions.

In Fig. 15 we directly compare three of the observed *n*-propanol curves with those predicted based on the continuum model described in Sec. II. In the case of *n*-propanol the continuum model predicts a multiexponential $C(t)$ with the long-time behavior being exponential and corresponding to the lowest frequency dispersion regime. This long component decays with a time constant approximately given by $\tau_{L1} = (\epsilon_{\infty 1}/\epsilon_{01})\tau_{D1}$. Shorter components in the response arise from the higher frequency parts of $\epsilon(\omega)$. For the calculation shown in Fig. 15, Eqs. (14)–(20) were used along with a fit of *n*-propanol dielectric data to a two Debye form. The parameters used in the calculations are given in the figure caption. Comparing the calculated and experimental curves it is clear that the measured $C(t)$ curves are nonexponential in a way quite different from the calculated ones. Whereas the calculated correlation functions are nonexponential only at early times, the experimental $C(t)$ curves are nonexponential at all times. This is especially clear in the 223 K curve in Fig. 15. In general we find that $C(t)$ decays more slowly than the calculated curves at long times.

Pronounced deviations from continuum theory predictions are observed for solvents with high dielectric constants ($\epsilon_0 > 50$), as shown by the data summarized in Table VI and in Fig. 16. For simplicity we compare only the average observed time constant $\langle\tau\rangle$ [Eq. (30)] to the longest longitudinal relaxation time of the solvent $\tau_L = \tau_{L1} = (\epsilon_{\infty 1}/\epsilon_{01})\tau_{D1}$. Such a comparison is only approximate since $\langle\tau\rangle$ may be shortened by contributions from $C(t)$ components resulting from high-frequency dispersions in $\epsilon(\omega)$. For the present purposes however using $\langle\tau\rangle = \tau_L$ as a rough gauge of agreement with continuum theory is adequate. In Fig. 16, $\langle\tau\rangle/\tau_L$ is plotted vs ϵ_0 on a logarithmic scale. The dashed line here represents the continuum theory prediction. At low to moderate ϵ_0 (< 50), the observed $\langle\tau\rangle$ are approximately equal to τ_L. For the largest dielectric constant solvents studied ($\epsilon_0 \sim 300$) the observed solvation time scale $\langle\tau\rangle$ is 15 times greater than τ_L and there appears to be a reasonable correlation between $\langle\tau\rangle/\tau_L$ and ϵ_0. Several points about Fig. 16 are worth noting. First, $\langle\tau\rangle$ varies over a factor of more than 20-fold in the region where $\langle\tau\rangle \cong \tau_L$. Second, the values of $\langle\tau\rangle$ for the high dielectric constant solvents, propylene carbonate and *n*-methyl propionamide lie in the middle of the range of $\langle\tau\rangle$ values. Further, the spectral shifts found in these two solvents fit with the other solvents very well (Fig. 3). Thus, the stabilization in the high dielectric constant solvents conforms to expectations, but it occurs *much more slowly* than continuum theory predicts.

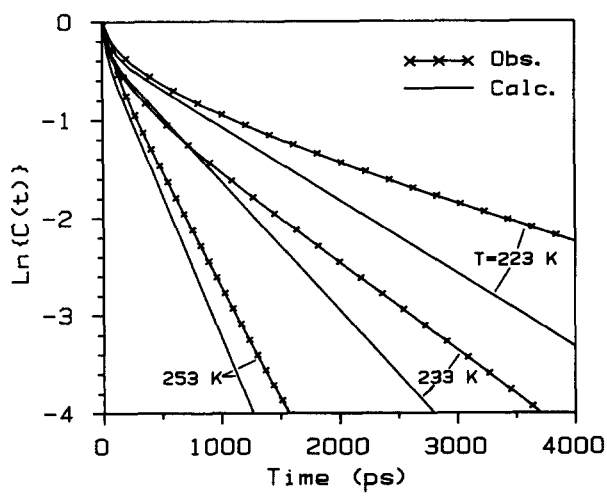

FIG. 15. Comparison of observed (×-×-×) and calculated (—) $C(t)$ correlation functions in *n*-propanol. The calculated curves were obtained using the continuum theory expressions [Eq. (14)–(20)] and approximating the *n*-propanol dielectric response by a two Debye form. The dielectric parameters used in these calculations were for 253, 233, and 223 K, respectively: $\epsilon_{01} = 27.81$, 31.43, and 33.80; $\epsilon_{\infty 1} = 3.94$, 4.10, and 4.20; $\epsilon_{\infty 2} = 3.10$, 3.14, and 3.16; $\tau_{D1} = 2140$, 5190, and 9600 ps; $\tau_{D2} = 12.3$, 19.7, and 28.3 ps.

TABLE VI. Dielectric dispersion parameters and average solvation times.

Solvent	T (K)	Dielectric parameters ϵ_{01}	$\epsilon_{\infty 1}$	τ_{D1}	$\tau_{L1}=\left(\frac{\epsilon_{\infty 1}}{\epsilon_{01}}\right)_{\tau_{D1}}$	Solvation $\langle\tau\rangle$[b]
Ethanol	253	32.4	4.86	643	96	112 ± 11
n-Propanol	295	21.1	3.67	438	77	59 ± 11
	273	24.2	3.80	934	140	138 ± 21
	251	27.8	3.94	2140	300	304 ± 46
	232	31.4	4.10	4960	650	661 ± 59
	221	33.8	4.20	9630	1200	1340 ± 270
n-Butanol	253	23.7	3.65	3220	500	479 ± 48
2-Propanol	253	26.4	3.70	3050	430	488 ± 53
N-methyl-propionamide	273	215	6	392	10	125 ± 25
	244	299	6	1890	40	545 ± 55
Propylene Carbonate	252	77.3	10	104	10	49 ± 10
	237	81.9	10	171	20	88 ± 13
	221	86.8	10	346	40	459 ± 46

[a] ϵ_{01}, $\epsilon_{\infty 1}$, and τ_{D1} refer to the lowest frequency dielectric dispersion range if more than one range exists (as for the alcohols). These data were generated from fits of temperature dependent dielectric measurements collected from the original literature. The fitting procedure and original references for the *n*-alcohols are given in M. Maroncelli and G. R. Fleming, in preparation. For *N*-methylpropionamide data were taken from S. J. Bass, W. I. Nathan, R. M. Meighan, and R. H. Cole, J. Phys. Chem. **68**, 509 (1964). For propylene carbonate values were obtained from: R. Payne and I. E. Theodorou, *ibid.* **76**, 2892 (1972); L. Simeral and R. L. Amey, *ibid.* **74**, 1443 (1970).

[b] Best experimental values of the average solvation time $\langle\tau\rangle$ [Eq. (30)]. These values were obtained from an average of several measurements from direct integration and from fitting the $C(t)$ data to various functional forms. The error limits indicate the standard deviation of the set of measurements.

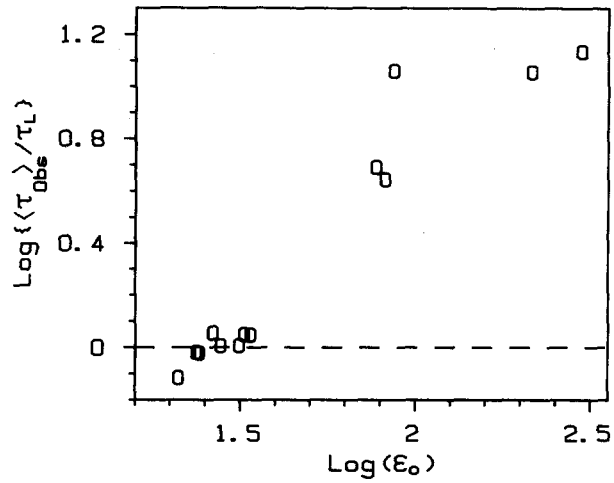

FIG. 16. Summary of solvation times observed for Cu153 compared to continuum theory predictions. The ratio of the average $C(t)$ time constant $\langle\tau\rangle$ (Table VI) observed to the predicted solvent longitudinal relaxation time $\tau_{L(1)}$ is plotted as a function of solvent dielectric constant. Logarithmic scales are used only to help spread out the data. The dashed line at $\log(\langle\tau\rangle/\tau_L)=0$ is the continuum prediction.

We, therefore, believe that the data in Fig. 16 point to a clear breakdown of the continuum picture at high ϵ_0 values. Interpretations of this behavior in terms of the molecularity of the solvent will be discussed in Sec. V.

A final aspect of the time-evolving spectra of interest is the fact that the spectrum changes shape slightly in time. As the most reliable measure of these changes we chose the bandwidth (FWHM) of the spectrum, Γ, determined from the parameters of the fitted log normal using Eq. (28). In all solvents studied, Γ was observed to be in the range 2800–3400 cm^{-1} and to decrease by 10%–20% between $t=0$ and $t=\infty$. By defining a correlation function $C_\Gamma(t)$ analogous to $C(t)$ as

$$C_\Gamma(t)\equiv\frac{\Gamma(t)-\Gamma(\infty)}{\Gamma(0)-\Gamma(\infty)}, \tag{34}$$

the temporal evolution of the spectral shape can be compared to that of the shift. Typical $C_\Gamma(t)$, $C(t)$ pairs are shown in Fig. 17 for the *N*-methylpropionamide solvent. In these examples, and in all cases studied, the width and shift correlation functions appear to show approximately the same time evolution.

The observed line shape changes partly reflect changes in the distribution of solvent environments. The situation can be described by referring again to Fig. 5. In our experiments the excitation wavelength is near to the maximum of the steady-state absorption spectrum. For this spectral region there is a continuum of vibronic transitions whose net intensity is essentially constant over the frequency spread produced by the environment distribution ($\sim 200^{-1}$). In such a case all molecules are excited simultaneously with a narrow frequency laser and the entire distribution of solvent environments initially present in S_0 (Fig. 5) is transferred unchanged into S_1 by the excitation at $t=0$. Assuming that vibrational relaxation in S_1 is much faster than the solvation time scale, the $t=$ "0" fluorescence should have essentially the same width as present in the steady-state absorption spectrum. The width should then increase with time to the steady-state fluorescence value. The picture only approximately coincides with the observed behavior. The $t=0$ widths we observe are actually already narrower than the

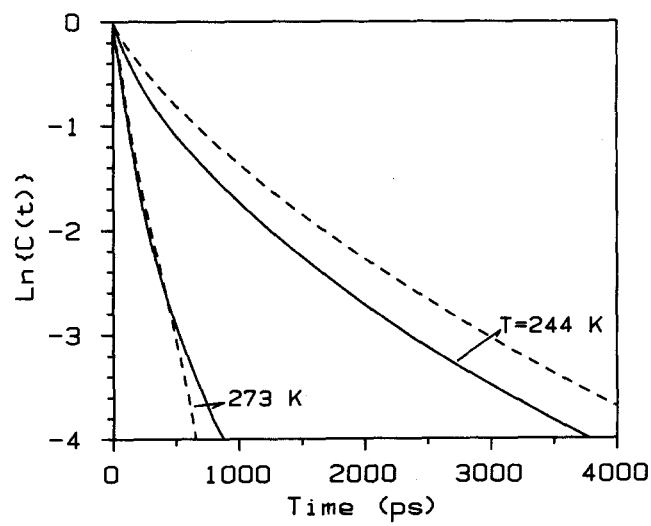

FIG. 17. Comparison of the temporal evolution of the spectral shape and average frequency. The solid curves are the $C(t)$ correlation functions constructed from average frequencies $\bar{\nu}(t)$ [Eq. (30)]. The dashed curves are an analogous correlation function $C_\Gamma(t)$ constructed using the width of the spectrum $\Gamma(t)$ rather than the frequency [Eqs. (28) and (34)]. These data are for *N*-methylpropionamide solvent at the indicated temperatures.

absorption widths. Further, Loring *et al.*[15] showed that under quite general conditions the above picture would predict $C_\Gamma(t)$ to decay with twice the rate of $C(t)$ rather than with roughly the same rate as we observed. Thus, the time-dependent width changes only partly reflect changes in the distribution of solvent environments. Other effects probably also contribute to the observed behavior.

V. DISCUSSION

The results we have obtained on the solvation behavior of Cu153 in polar solutions may be summarized as follows:

(i) Steady-state studies show that the absorption and fluorescence spectra of Cu153 are good measures of polar solvation. In polar aprotic solvents spectral frequencies are linearly related to solvent polarity (Figs. 3 and 4). Based on these shifts and results of semiempirical calculations we estimate a dipole moment of ~ 10 D in the S_1 state compared to ~ 5.6 D in S_0. Cu153 does form specific hydrogen bonds with H-bond donors such as alcohols and this effect causes a (smaller) additional shift in the spectrum over that due just to solvent polarity.

(ii) The rotational dynamics of Cu153 are anomalous. In addition to the normal diffusive rotation expected for a molecule of its size and shape, the fluorescence anisotropy decay exhibits an extra, fast component. We interpret this fast component as being due to a time-dependent rotation of the transition dipole which occurs in response to changing solvent environment; i.e., the S_1 electronic state in Cu153 is somewhat sensitive to solvation state. In support of this interpretation we note that the time constant for this fast rotation is correlated to the spectral shift (solvation) times as a function of solvent. Further, the anomalous changes in fluorescence bandwidths in both steady-state and time-dependent spectra are consistent with minor changes in the vibronic structure of S_1 with polarity. Thus solvation of Cu153 has some feedback character to it. The large dipole of the S_1 state polarizes its surroundings which, in turn, react back to slightly modify the S_1 charge distribution. Energetically, such a scenario is quite reasonable. Based on a continuum calculation like the one used in Sec. IV B, solvent stabilization of the S_1 dipole (10 D) is calculated to be 10 000 cm^{-1} in a solvent with $\epsilon_0 = 50$ (DMSO). The S_0--S_1 transition energy is 25 000 cm^{-1} so that the solvation energy is substantial relative to the electronic energy of the isolated solute. It would be surprising if the probe remained entirely unaffected by this strong interaction with its environment. These energetics are not unique to Cu153 but also apply to many other highly polar probes used in spectral shift studies. It is possible that the effects observed here for Cu153 are a general feature of such systems which have previously gone unnoticed.[44]

(iii) The solvation dynamics observed for Cu153 in a variety of solvents show marked deviations from predictions based on continuum theories. The observed $C(t)$ correlation functions show that relaxation of the solvent occurs on multiple time scales in a manner not consistent with continuum predictions. For the solvents studied here, except at short times, a single exponential decay of $C(t)$ with time constant equal to the solvent longitudinal relaxation time τ_L ($=\tau_{L1}$) is predicted. We observe relaxation components with much longer time constants than τ_L. In solvents with static dielectric constants $\epsilon_0 < 50$ we observe, partly fortuitously, that the *average* time constant $\langle\tau\rangle$ for solvation is approximately equal to τ_L. For the solvents propylene carbonate and *N*-methylpropionamide, which have $\epsilon_0 \gg 50$, $\langle\tau\rangle$ is much greater than τ_L. The ratio $\langle\tau\rangle/\tau_L$ seems to be correlated with solvent dielectric constant (Fig. 16).

It is useful to compare the results obtained with other probe molecules to those found here with Cu153. Overall, where direct comparison is possible, there is reasonable agreement with the above picture. In a number of early studies Brand *et al.*[45] measured $C(t)$ functions for several anilinonaphthalenes in glycerol. Glycerol possesses a non-Debye dielectric response which does not allow for an analytical description of the spectral shift in a continuum model. Comparing numerically calculated $C(t)$ curves[46] based on the continuum model with the observed results shows that solvation dynamics are much slower than predicted. This might be expected based on our results since $\epsilon_0 = 40$–60 at the temperatures studied. We must note however that given the available time resolution, for the nonexponential $C(t)$ predicted, comparison with experiment is quite uncertain due to difficulty in assigning $\bar{\nu}(0)$. Barbara *et al.*[43] have recently studied three probe molecules in the weakly polar ($\epsilon_0 \sim 7$) solvent triacetin which has a non-Debye dielectric response similar to that of glycerol. These authors show that depending on their method for choosing $\bar{\nu}(0)$, the nonexponential $C(t)$ functions observed appear to decay either more or less rapidly than predicted. In solvents which show simpler dielectric functions, comparison with theory is more straightforward. Our own study of the probe LDS-750[16] yielded values of $\langle\tau\rangle/\tau_L$ near unity for several polar aprotic solvents although in methanol the value was much lower (0.3). In general nonexponential $C(t)$ curves were observed. Except for the apparently anomalous results of Rulliere *et al.*,[47] studies of other probes in the *n*-alcohols ethanol through pentanol, have yielded results similar to ours for Cu153. For example, Safar–Zedeh–Amiri examined the probe *trans*-4-dimethyl-amino-4'-cyanostilbene in *n*-butanol between 250 and 300 K.[48] Although he did not record the full spectral movement, the results showed the shift times to be approximately equal to τ_L over this temperature range. Yeh *et al.*[49,50] determined $C(t)$ functions for the probe 4-aminophthalimide in several alcohols near room temperature. These authors also observed spectral shift times approximately equal to τ_L. Further their $C(t)$ curves[50] are clearly nonexponential. Finally, we have also measured $C(t)$ functions in alcohols (250 K) using the probe 1-aminonaphthalene.[51] While not identical, the $C(t)$ curves with this probe are similar in average time constant and in nonexponentiality to the corresponding results with Cu153.

We believe that the results obtained with the probe Cu153 allow for some general conclusions concerning solvation dynamics. In particular, we interpret the poor agreement of our observed $C(t)$ functions with continuum-based predictions as reflecting the importance of the molecularity of the solvent in determining solvation rates. This failure of the continuum description is of a universal nature and does not depend on any peculiarities of the particular solute or

specific solute–solvent interactions in the system we have chosen. Having said this we must now address two objections which could be raised against the generality of our results. First, we have evidence that there is electronic redistribution taking place in the excited state during solvation. The theoretical description of solvation outlined in Sec. II considers the solute to be unaffected by its solvation state. The more complex probe–solvent interaction occurring in the experimental system might be expected to complicate the observed dynamics. While this is likely to be true, the magnitude of the effect must be small in the present case. A large change in, for example, the magnitude of the S_1 dipole as a function of polarity would manifest itself as a nonlinear dependence of the steady-state fluorescence shifts with polarity, contrary to experiment. Further, experiments with 1-aminonaphthalene as a probe in several alcohols[51] show quite similar $C(t)$ correlation functions to those observed with Cu153. Thus, the changes in the S_1 state, while interesting, probably do not alter the observed solvation dynamics in a substantial way.

The second objection is more serious and has to do with the fact that Cu153 forms hydrogen bonds with H-bond donating solvents. Due to limited time resolution, most of our studies have been performed with such solvents. One must question whether the observed deviations from continuum predictions are not just due to hydrogen bonding dynamics. While hydrogen bonding is an important aspect of solvation, it is a complication preferably avoided until the (simpler) nonspecific dipolar aspects of solvation are examined. Clearly, the continuum models described in Sec. II are not intended to account for specific solute–solvent interactions like hydrogen bonding. Two facts argue strongly against hydrogen bonding effects being the principle cause of the observed deviations. First, the trend of $\langle\tau\rangle/\tau_L$ shown in Fig. 16 seems to be correlated with ϵ_0 and not with hydrogen bonding ability. Thus, *N*-methylpropionamide is similar to the *n*-alcohols in its H-bond donating properties yet there is a dramatic difference in their dynamics. More convincingly, propylene carbonate also seems to fit into the above correlation. Propylene carbonate is a nonassociated solvent which has *no* hydrogen-bond donating capabilities, yet we see the same sort of nonexponential $C(t)$ decays and larger $\langle\tau\rangle/\tau_L$ ratios in this solvent than we do with the alcohols. We conclude then that, although specific hydrogen bonds to the solute are present in many of the solvents studied, these interactions do not account for most of the discrepancy between the observed solvation dynamics and the behavior predicted from continuum theories.

What then is causing continuum models to fail in the description of solvation dynamics? We believe the answer is that during the solvent relaxation process the solute senses the molecularity of its environment. In the continuum picture, the surrounding medium relaxes with a characteristic time constant τ_L, the solvent longitudinal relaxation time. τ_L is not a single-molecule property but rather a macroscopic quantity characteristic of the collective response of many molecules. It is related to the more nearly single-particle reorientation time τ_D by $\tau_L = (\epsilon_\infty/\epsilon_0)\tau_D \ll \tau_D$. The continuum description of solvation requires that all contributions to the solvation energy, coming from regions both near to and far from the solute, respond with this faster-than-molecular time constant τ_L. A simple calculation, based on the continuum desciption itself, shows that such an expectation is unrealistic for solutes of moderate size. In a continuous dielectric medium the polarization per unit volume surrounding a dipolar solute decreases as $1/r^3$ where r is the distance from the dipole. Similarly the interaction energy between the dipole and this polarization decreases as $1/r^6$. On this basis, for a solute of radius $a = 3.9$ Å such as Cu153, 50% of the solute–solvent interaction energy is obtained from a region $r \leqslant 5.0$ Å. At solvent densities typical of methanol or DMSO, such a solvation shell would on average contain only two to four solvent molecules! This crude calculation illustrates the fact that a large part of the solvation response is due to a relatively small number of nearest neighbor solvent molecules, even if only dipolar interactions are considered. As a result, we should not expect a continuum description of the dynamics to be entirely appropriate. The part of the response coming from regions far removed from the solute should look continuum-like. Here, the response will be due to the collective reaction of many solvent molecules and should contribute a fast τ_L component to the response. Near the solute, however, solvation comes about through movement of individual solvent molecules, and, therefore, takes place on a time scale much slower than τ_L and more closely related to τ_D. This behavior was first predicted by Onsager in his cryptic "snowball" comment concerning electron solvation[52] and has recently been observed in computer simulations of solvation in water.[53] As a result, the overall solvation dynamics should show multiple time scale relaxations in the range between τ_L and τ_D, which is just what we observe experimentally. Further, since the single-particle contributions to the relaxation are always present, the observed $\langle\tau\rangle$ should show poorer and poorer agreement with τ_L as ϵ_0 gets larger, i.e., as τ_L and τ_D become more and more dissimilar. The experimental trend illustrated by Fig. 16 is therefore reasonable.

To proceed further than the above qualitative description, more molecularly based theories of solvation dynamics are needed. Progress along these lines has been made by Calef and Wolynes[54] and most recently Wolynes.[20] Calef and Wolynes[54] studied the problem of ionic solvation using a mean field Smoluchowski–Vlasov approach. Numerical solution of the resulting integral equations yielded results for charge solvation in methanol and ethanol. While not directly comparable to our results, the calculated $C(t)$ functions are qualitatively similar to those we observe. Both are nonexponential with average time constants greater than τ_L. In a second approach, Wolynes[20] has obtained a partial analytical solution of a molecular theory of solvation in the mean spherical approximation. For solvation of a ion of radius a, Wolynes finds that in addition to τ_L a second relaxation time τ_G given by

$$\tau_G = \left\{\frac{1 + (1/4)(a/b)(\epsilon_\infty + 3)}{1 + (1/4)(a/b)(\epsilon_0 + 3)}\right\}\tau_D \tag{35}$$

is relevant to the solvation dynamics. In this expression b is the solvent radius. There is actually a continuum of relaxa-

tion times involved but in rough approximation the response is biexponential with time constants τ_L and τ_G. The latter time constant can be loosely associated with the time for structural rearrangement of the first solvation shell about the ion.[20] Again we cannot compare this result to our experiment directly, however, τ_G shows suggestive trends with ϵ_0. Using parameters $\epsilon_\infty = 1$ and the solute/solvent size ratio $a/b = 1$, Eq. (35) predicts (τ_G/τ_L) to be a monotonically increasing function of ϵ_0 with $(\tau_G/\tau_L) = 1$ at $\epsilon_0 = 1$ and asymptotically approaching the value 8 as $\epsilon_0 \to \infty$. This trend is reminiscent of the observed correlation between $\langle\tau\rangle/\tau_L$ and ϵ_0. The physical basis of this seems to be that as ϵ_0 increases the contribution of more and more molecules is required to reduce τ_D to τ_L. If τ_G refers to roughly the first solvation shell, when more molecules than are contained in this shell are required to give the full τ_L response, τ_G will become longer than τ_L. Eq. (35) also shows that τ_G decreases (becomes more like τ_L) as the solute/solvent size ratio increases. In the limit $a/b \to \infty$ the continuum result $\tau_G = \tau_L$ should pertain although this is not quite true at the level of approximation of Eq. (35). The theory thus predicts that some size dependence of both the probe and solvent might be observable.

In conclusion, we have examined solvation dynamics in a number of solvents using the probe Cu153. We have observed what we believe is a general lack of agreement between the observed dynamics and expectations based on continuum theories of solvation. Theories which begin from a molecular description appear to be necessary in order to fully understand solvation dynamics. Such theories are beginning to emerge but further work on both the theoretical and experimental fronts is needed before molecularly based theories can be adequately tested.

ACKNOWLEDGMENTS

This work was supported by grants from the National Science Foundation. We thank S. P. Webb and E. W. Castner, Jr. for their assistance and P. G. Wolynes for communication of his theoretical work prior to publication.

APPENDIX

The most explicit theoretical treatments of the time-dependent Stokes shift based on a continuum solvent/point dipole model have been described in two papers by Bagchi, Oxtoby, and Fleming[13] (BOF) and by Mazurenko.[12] While the model employed in these two papers is essentially identical, the results are slightly different due to what we believe is a minor error in the Bagchi formulation. In this Appendix we show how a correction of this error leads to complete agreement between these formulations and that of van der Zwan and Hynes.[14]

Both treatments represent the solute by a spherical cavity of radius a having a centered point dipole moment μ_0. The solute polarizability α is introduced explicitly by Mazurenko and indirectly in the BOF treatment by means of an (infinite frequency) dielectric constant ϵ_c, within the solute cavity. Both treatments begin by deriving expressions for the interaction energy of such a solute in equilibrium with a surrounding continuum fluid of dielectric constant ϵ_0. The equilibrium result is then generalized into the time domain via a quasistatic replacement of ϵ_0 by $\epsilon(\omega)$. The difference between the two methods occurs at the very outset in the expression of the equilibrium reaction fields and energies.

In the BOF treatment, the interaction energy of the solute and its surroundings, ΔE, is written in terms of a reaction field $\mathbf{R}$ and the solute parameters μ_0 and ϵ_c as[13]:

$$\Delta E = -\mu_0 \cdot \mathbf{R} = -\tfrac{1}{2}(\epsilon_c + 2)\mu_v \cdot \mathbf{R}, \tag{A1}$$

$$\mathbf{R} = \frac{2}{\epsilon_c a^3}\left(\frac{\epsilon_0 - \epsilon_c}{2\epsilon_0 + \epsilon_c}\right)\left(\frac{\epsilon_c + 2}{3}\right)\mu_v, \tag{A2}$$

$$\mu_v = \left(\frac{3}{\epsilon_c + 2}\right)\mu_0. \tag{A3}$$

Equation (A2) is a standard result for the reaction field inside the solute cavity.[55] In choosing to work with the ϵ_c rather than α directly the BOF treatment introduces the screened moment μ_v defined by Eq. (A3). This is the so-called "external moment"[55] which would be measured for this model solute in the gas phase. (Ref. 13 denotes μ_v as simply μ.) μ_v rather than μ_0 is to be associated with the solute's dipole moment and it is the quantity equivalent to μ_0 in the Mazerenko formulation. The error in these equations is evident from the fact that ΔE does not vanish for $\epsilon_0 = 1$, i.e., for the isolated solute. The above reaction field includes both the effect of the solute polarizing its surroundings (ϵ_0) as well as the effect of the molecule polarizing itself through ϵ_c.[56] To correct this feature we should really consider only that part of the reaction field not present for the solute *in vacuo*. $\mathbf{R}$ should be replaced by $\mathbf{R}'$ given by

$$\mathbf{R}' = \mathbf{R}(\epsilon_0) - \mathbf{R}(\epsilon_0 = 1) = \frac{2}{a^3}\left(\frac{\epsilon_0 - 1}{2\epsilon_0 + \epsilon_c}\right)\mu_v. \tag{A4}$$

With this modification the solvation energy then becomes

$$\Delta E = \frac{-2}{a^3}\left(\frac{\epsilon_0 - 1}{2\epsilon_0 + \epsilon_c}\right)\left(\frac{\epsilon_c + 2}{3}\right)\mu_v^2. \tag{A5}$$

Mazerenko chooses to use the solute polarizability α rather then ϵ_c. The derivation of equations analogous to Eq. (A1)–(A3) is somewhat more transparent in this case and yields[12]

$$\Delta E = -\mu_0 \cdot \mathbf{R}, \tag{A6}$$

$$\mathbf{R} = \frac{2}{a^3}\left(\frac{\epsilon_0 - 1}{2\epsilon_0 + 1}\right)(\mu_0 + \alpha\mathbf{R}), \tag{A7}$$

or

$$\mathbf{R} = \frac{2}{a^3}\left\{\frac{(\epsilon_0 - 1)}{(2\epsilon_0 + 1) - 2(\epsilon_0 - 1)\alpha/a^3}\right\}\mu_0. \tag{A8}$$

To compare these expressions to the BOF results α can be related to ϵ_c via the Clausius–Mossotti relationship

$$\alpha/a^3 = \left(\frac{\epsilon_0 - 1}{\epsilon_0 + 2}\right). \tag{A9}$$

$\mathbf{R}$ can be written in terms of ϵ_c as

$$\mathbf{R} = \frac{2}{a^3}\left(\frac{\epsilon_0 - 1}{2\epsilon_0 + \epsilon_c}\right)\left(\frac{\epsilon_c + 2}{3}\right)\mu_0. \tag{A10}$$

Substituting Eq. (A10) into Eq. (A6) and making the association between μ_v (BOF) and μ_0 (Mazerenko), a result identical to the modified BOF expression for ΔE [Eq. (A4)] is obtained.

The changes to be made in the later results of the BOF paper due to the correction described above are relatively minor. The generalized frequency-dependent reaction field $R(\omega)$ [Eqs. (2.2) and (2.3) of Ref. 13] becomes

$$\mathbf{R}(\omega) = \frac{2}{a^3}\left[\frac{\epsilon(\omega)-1}{2\epsilon(\omega)+\epsilon_c}\right]\left(\frac{\epsilon_c+2}{3}\right)\boldsymbol{\mu}_v(\omega), \qquad \text{(A11)}$$

where $\epsilon(\omega)$ is the frequency dependent dielectric function of the surroundings. For a single Debye $\epsilon(\omega)$ [Eq. (5) in the text] the pulse response function $r(t)$ [Eq. (2.6) in Ref. 13] is now

$$r(t) = G\delta(t) + Fe^{-t/\tau_F}, \qquad \text{(A12)}$$

$$G = \frac{2}{3a^3}\frac{(\epsilon_\infty - 1)}{(2\epsilon_\infty + \epsilon_c)}, \qquad \text{(A13)}$$

$$F = \frac{2}{a^3}\frac{(\epsilon_0 - \epsilon_\infty)(\epsilon_c + 2)}{(2\epsilon_\infty + \epsilon_c)^2}, \qquad \text{(A14)}$$

$$\tau_F = \left(\frac{2\epsilon_\infty + \epsilon_c}{2\epsilon_0 + \epsilon_c}\right)\tau_D. \qquad \text{(A15)}$$

The changes in $R(\omega)$ only affect the instantaneous part of the response $G\delta(t)$, which is not actually included in the $r(t)$ expression in the BOF paper. The experimentally observable part of the response (i.e., the second term) however is identical to that given by BOF, and this identity is independent of tha actual form of $\epsilon(\omega)$. Thus, the main results derived by BOF concerning $C(t)$ and the observable time dependence of the fluorescence Stokes shift are still applicable. The time-zero shifts and thus the steady-state shifts [for example, in Eqs. (3.12) and (3.15) in Ref. 13] are in error and the expressions given in the theoretical section should be used in favor of the BOF results. Of course for $\epsilon_c = 1$ the differences disappear and all of these expressions become equivalent.

[1] J. P. Bergsma, B. J. Gertner, K. R. Wilson, and J. T. Hynes, J. Chem. Phys. **86**, 1356 (1987).
[2] L. D. Zusman, Chem. Phys. **49**, 295 (1980).
[3] D. F. Calef and P. G. Wolynes, J. Phys. Chem. **87**, 3387 (1983); J. Chem. Phys. **78**, 470 (1983).
[4] J. T. Hynes, J. Phys. Chem. **90**, 3701 (1986).
[5] H. Sumi and R. A. Marcus, J. Chem. Phys. **84**, 4894 (1986).
[6] M. J. Weaver and T. Gennett, Chem. Phys. Lett. **113**, 213 (1985).
[7] M. McGuire and G. McLendon, J. Chem. Phys. **90**, 2549 (1986).
[8] E. M. Kosower and D. Huppert, Annu. Rev. Phys. Chem. **37**, 127 (1986), and references therein.
[9] See, for example, N. Mataga and T. Kubota, *Molecular Interactions and Electronic Spectra* (Dekker, New York, 1970), Chap. 8.
[10] W. Ware, S. K. Lee, G. J. Brant, and P. P. Chow, J. Chem. Phys. **54**, 4729 (1971); S. Chakrabarti and W. Ware, *ibid.* **55**, 5494 (1971).
[11] N. G. Bakshiev, Opt. Spectrosc. (USSR) **16**, 446 (1964); N. G. Bakshiev, Yu. T. Mazurenko, and I. V. Piterskaya, *ibid.* **21**, 307 (1966).
[12] Yu. T. Mazurenko, Opt. Spectrosc. (USSR) **36**, 283 (1974).
[13] B. Bagchi, D. W. Oxtoby, and G. R. Fleming, Chem. Phys. **86**, 257 (1984).
[14] G. van der Zwan and J. T. Hynes, J. Phys. Chem. **89**, 4181 (1985).
[15] R. F. Loring, Y. J. Yan, and S. Mukamel, Chem. Phys. Lett. (submitted); see also Y. T. Mazurenko, Opt. Spectrosc. (USSR) **48**, 388 (1980).
[16] E. W. Castner, Jr., M. Maroncelli, and G. R. Fleming, J. Chem. Phys. **86**, 1090 (1987).
[17] G. A. Reynolds and K. H. Drexhage, Opt. Commun. **13**, 222 (1975).
[18] R. F. Kubin and A. N. Fletcher, Chem. Phys. Lett. **99**, 49 (1983).
[19] G. Jones II, W. R. Jackson, S. Kanoktanaporn, and A. M. Halpern, Opt. Comun. **33**, 315 (1980); G. Jones II, W. R. Jackson, C. Choi, and W. R. Bergmark, J. Phys. Chem. **89**, 294 (1985).
[20] P. G. Wolynes (to be submitted).
[21] E. Lippert, Z. Naturforsch, Teil A **10**, 541 (1955); Z. Electrochem. **61**, 962 (1957).
[22] N. Mataga, Y. Kaifu, and M. Koizumi, Bull. Chem. Soc. Jpn. **29**, 465 (1956).
[23] E. G. McRae, J. Phys. Chem. **61**, 562 (1957).
[24] Many of the variants and their merits are discussed in B. Koutek, Coll. Czech. Chem. Commun. **43**, 2368 (1978); J. E. Brady and P. W. Carr, J. Phys. Chem. **89**, 5759 (1985).
[25] M. C. Chang, S. H. Courtney, A. J. Cross, R. J. Gulotty, J. W. Petrich, and G. R. Fleming, Anal. Instrum. **14**, 433 (1985).
[26] P. Bado, C. Dupuy, K. R. Wilson, R. Boggy, J. Bowen, and S. Westra, Opt. Commun. **46**, 241 (1983).
[27] A. J. Cross and G. R. Fleming, Biophys. J. **46**, 45 (1984).
[28] Only a few such calculations for Coumarin derivatives have been published: V. K. Ahuja, K. L. Kapoor, and N. K. Ray, Ind. J. Chem. **11**, 458 (1973); R. H. Abu-Eittah and B. A. H. El-Tawil, Can. J. Chem. **63**, 1173 (1985). See also Refs. 19 and 35.
[29] Available from the Quantum Chemistry Program Exchange (Chemistry Dept., Indiana University) as QCPE Program No. 506 (1985).
[30] M. J. S. Dewar and W. Thiel, J. Am. Chem. Soc. **99**, 4899 (1977).
[31] M. J. S. Dewar and W. Thiel, J. Am. Chem. Soc. **99**, 4907 (1977).
[32] T. Clark, *A Handbook of Computational Chemistry* (Wiley, New York, 1985).
[33] J. Sadlej, *Semi-Empirical Methods of Quantum Chemistry*, translated by I. L. Cooper (Ellis Horwood, Chichester, 1985).
[34] V. S. Griffiths and J. B. Westmore, J. Chem. Soc. **1963**, 4941.
[35] W. Rettig and A. Klock, Can. J. Chem. **63**, 1649 (1985).
[36] N. P. Ernsting, M. Asimov, and F. P. Schafer, Chem. Phys. Lett. **91**, 231 (1982).
[37] M. J. Kamlet, J. L. M. Abboud, and R. W. Taft, Prog. Phys. Org. Chem. **13**, 485 (1981).
[38] C. Reichardt, in *Molecular Interactions*, edited by H. Ratajczak and W. J. Orville-Thomas (Wiley, New York, 1981), Vol. 3, p. 241.
[39] G. R. Fleming, *Chemical Applications of Ultrafast Spectroscopy* (Oxford, London, 1986), Chap. 6.
[40] A. Bondi, J. Phys. Chem. **68**, 441 (1964); J. T. Edwards, J. Chem. Ed. **47**, 261 (1970).
[41] D. B. Siano and D. E. Metzler, J. Chem. Phys. **51**, 1856 (1969).
[42] For recent interpretations of the physical meaning of this functional form see M. F. Shlesinger and E. W. Montroll, Proc. Natl. Acad. Sci. U.S.A. **81**, 1280 (1984); R. G. Palmer, D. L. Stein, E. Abrahams, and P. W. Anderson, Phys. Rev. Lett. **53**, 958 (1984).
[43] V. Nagarajan, A. M. Brearley, T.-J. Kang, and P. F. Barbara, J. Chem. Phys. (in press, 1987).
[44] Solvent induced changes in transition dipole direction have been previously noted for solutes with very weakly allowed transitions. See, for example, F. W. Langkilde, E. W. Thulstrup, and J. Michl, J. Chem. Phys. **78**, 3372 (1983), and references therein.
[45] R. P. DeToma, J. H. Easter, and L. Brand, J. Am. Chem. Soc. **98**, 5001 (1976); R. P. DeToma and L. Brand, Chem. Phys. Lett. **47**, 231 (1976); A. Gafni, R. P. DeToma, R. E. Manrow, and L. Brand, Biophys. J. **17**, 155 (1977).
[46] M. Maroncelli and G. R. Fleming (unpublished results).
[47] C. Rulliere, A. Declemy, and Ph. Kottis, in *Ultrafast Phenomena V*, edited by G. R. Fleming and A. E. Siegman (Springer, Berlin, 1986), p. 312.
[48] A. Safarzadeh-Amiri, Chem. Phys. Lett. **215**, 272 (1986).
[49] S. W. Yeh, L. A. Philips, S. P. Webb, L. F. Buhse, and J. H. Clark, in *Ultrafast Phenomena IV*, edited by D. H. Auston and K. B. Eisenthal (Springer, Berlin, 1984), p. 359.
[50] S. W. Yeh, Ph.D. thesis (1985), University of California, Lawrence Berkeley Laboratory Publication No. LRL-20662.
[51] M. Maroncelli, S. P. Webb, and G. R. Fleming (unpublished results).
[52] L. Onsager, Can. J. Chem. **55**, 1819 (1977).
[53] M. Maroncelli, E. W. Castner, Jr., S. P. Webb, and G. R. Fleming, in *Ultrafast Phenomena V*, edited by G. R. Fleming and A. E. Siegman (Springer, Berlin, 1986), p. 303.
[54] D. F. Calef and P. G. Wolynes, J. Chem. Phys. **78**, 4145 (1983).
[55] See, for example, H. Frohlich, *Theory of Dielectrics* (Oxford, London, 1958), especially Appendix A2.
[56] The same error also occurs in T.-W. Nee and R. Zwanzig, J. Chem. Phys. **52**, 6353 (1970).